

1 **Comparative and Integrated Analysis of Plasma Extracellular Vesicles Isolations**

2 **Methods in Healthy Volunteers and Patients Following Myocardial Infarction**

3 **Short title:** Integrated Analysis of Plasma Extracellular Isolation Methods

4 Daan Paget^{1,2}, Antonio Checa³, Benedikt Zöhrer^{4,5}, Raphael Heilig⁶, Mayooran
5 Shanmuganathan^{1,7}, Raman Dhaliwal⁸, Errin Johnson⁸, Maléne Møller Jørgensen^{9,10}, Rikke
6 Bæk⁹, Oxford Acute Myocardial Infarction Study (OxAMI)^{1,7}, Craig E. Wheelock^{3,5,11}, Keith M.
7 Channon^{1,7}, Roman Fischer⁶, Daniel C. Anthony², Robin P. Choudhury^{1,7} and Naveed
8 Akbar¹.

9 ¹ Division of Cardiovascular Medicine, Radcliffe Department of Medicine, University of
10 Oxford, Oxford, United Kingdom.

11 ² Department of Pharmacology, University of Oxford, Oxford, United Kingdom.

12 ³ Unit of Integrative Metabolomics, Institute of Environmental Medicine, Karolinska Institute,
13 Stockholm, Sweden.

14 ⁴ Respiratory Medicine Unit, Department of Medicine Solna and Center for Molecular
15 Medicine, Karolinska Institutet, Stockholm, Sweden.

16 ⁵ Department of Respiratory Medicine and Allergy, Karolinska University Hospital,
17 Stockholm, Sweden.

18 ⁶ Target Discovery Institute, Centre for Medicines Discovery, Nuffield Department of
19 Medicine, University of Oxford, Oxford, United Kingdom.

20 ⁷ Acute Vascular Imaging Centre, Radcliffe Department of Medicine, University of
21 Oxford, United Kingdom.

22 ⁸ Sir William Dunn School of Pathology, University of Oxford, Oxford, United Kingdom.

23 ⁹ Department of Clinical Immunology, Aalborg University Hospital, Aalborg, Denmark.

24 ¹⁰ Department of Clinical Medicine, Aalborg University, Aalborg, Denmark.

25 ¹¹ Gunma University Initiative for Advanced Research (GIAR), Gunma University, Showa-
26 machi, Maebashi, Gunma, Japan.

27

28 **Word Count: 11,258**

29 **Number of Figures: 8**

30 ***Corresponding Author:** Dr Naveed Akbar

31 **E-mail:** Naveed.Akbar@cardiov.ox.ac.uk

32 Telephone Number: 01865 234902

33 Address: Division of Cardiovascular Medicine, Radcliffe Department of Medicine, John
34 Radcliffe Hospital, Level 6, West Wing, OX3 9DU, United Kingdom.

35

36

37 **Abstract**

38 Plasma extracellular vesicle (EV) number and composition are altered following myocardial
39 infarction (MI), but to properly understand the significance of these changes it is essential to
40 appreciate how the different isolation methods affect EV characteristics, proteome and
41 sphingolipidome. Here, we compared plasma EV isolated from platelet-poor plasma from
42 four healthy donors and six MI patients at presentation and 1-month post-MI using
43 ultracentrifugation, polyethylene glycol precipitation, acoustic trapping, size-exclusion
44 chromatography (SEC) or immunoaffinity capture. The isolated EV were evaluated by
45 Nanoparticle Tracking Analysis, Western blot, transmission electron microscopy, an EV-
46 protein array, untargeted proteomics (LC-MS/MS) and targeted sphingolipidomics (LC-
47 MS/MS). The application of the five different plasma EV isolation methods in patients
48 presenting with MI showed that the choice of plasma EV isolation method influenced the
49 ability to distinguish elevations in plasma EV concentration following MI, enrichment of EV-
50 cargo (EV-proteins and sphingolipidomics) and associations with the size of the infarct
51 determined by cardiac magnetic resonance imaging 6 months-post-MI. Despite the selection
52 bias imposed by each method, a core of EV associated proteins and lipids was detectable
53 using all approaches. However, this study highlights how each isolation method comes with
54 its own idiosyncrasies and makes the comparison of data acquired by different techniques in
55 clinical studies problematic.

56

57 **Key words**

58 Ultracentrifugation, size exclusion chromatography, precipitation, acoustic trapping,
59 immunoaffinity capture, plasma, omics, human.

60

61 **Introduction**

62 Plasma extracellular vesicles (EV) are increased in number and carry altered protein, lipid
63 and RNA cargo in the peripheral blood in many pathologies [1-6]. Analysis of plasma EV by
64 omics approaches may provide unparalleled insight into multiple disease mechanisms and
65 disease monitoring in patients for personalized medicine. However, it is unclear how different
66 plasma EV isolation methods influence the plasma EV-profile or the so-called 'EV-signature'
67 in patients.

68

69 Current methods for the isolation of heterogeneous plasma EV include: ultracentrifugation
70 (UC), density ultracentrifugation, field-flow fractionation, size-exclusion chromatography
71 (SEC), precipitation, acoustic trapping [7] and immunoaffinity capture [8]. However,
72 unsurprisingly, laborious protocols that yield pure EV from plasma are less well favoured in
73 large cohorts [9, 10] than protocols that are easier, lower cost, and more convenient. These
74 methodological predilections are further impacted by the availability of stored biobank
75 plasma, which often carry contaminating erythrocytes, immune cells, and platelets [11].
76 Irrespective of pre-storage processing, all plasma is a rich source of lipoproteins
77 (apolipoprotein A and B), albumin, globulins and fibrinogens, which can co-isolate with
78 plasma EV. The proportion of these cell-derived and non-cellular contaminants in the purified
79 sample is method-dependent [12] and they may obscure EV associated cargo [13, 14].

80

81 Comparative isolation studies for plasma EV often assess EV size and concentration by
82 Nanoparticle Tracking Analysis (NTA) and morphology by transmission electron microscopy
83 (TEM). EV markers are usually evaluated using western blot or flow cytometry [15-18] .
84 These standard analyses are often driven by the requirements of scientific bodies and
85 consensus statements, which might be considered too prescriptive and refractory to change
86 as our understanding of EV biology evolves [14]. However, additional assessments of how
87 isolation methods influence the plasma EV preparation have been explored with a range of
88 techniques, including proteomics [16, 18-21], profiling of cytokines [22], RNA integrity [23,

89 24], lipidomics [25], flow cytometry [15, 26] or a combination of these methods [16].
90 However, the wide range of plasma EV isolation and characterization techniques has
91 evolved largely in the absence of systematic method characterization comparisons. As a
92 consequence, the absence of an understanding of the impact of isolation techniques has led
93 to plenty of uncertainty in relation to the interpretation of EV discoveries in clinical samples.

94

95 Here, we used platelet-free plasma from the same healthy volunteers to compare five
96 different plasma EV isolation methods including: UC, precipitation, acoustic trapping, SEC
97 and immunoaffinity capture using tetraspanins CD9, CD63 and CD81 (**Figure 1**). We then
98 sought to determine how plasma EV isolation methods influence EV characteristics in a set
99 of clinically well characterised individuals. Acute myocardial infarction (MI) is an important
100 pathology; it is also an example of sterile inflammation where plasma EV number and
101 composition are acutely altered [5, 6]. Plasma EV from MI patients at two different time
102 points were isolated using the five different EV isolation methods (**Figure 1**). Integrated
103 unsupervised analysis of all the acquired characterization data from the five different
104 methods was used to identify the similarities and differences between each method and to
105 highlight how each technique might influence the protein and sphingolipid composition.

106 **Materials and Methods**

107 Healthy Volunteers and Acute Myocardial Infarction Patients.

108 All human investigations were conducted in accordance with the Declaration of Helsinki. The
109 Oxfordshire Research Ethics Committee (Ref: 08/H0603/41 and 11/SC/0397) approved the
110 human clinical protocols. All healthy volunteers and myocardial Infarction (MI) patients
111 provided informed written consent for inclusion in the study.

112

113 Generation of Platelet Poor Plasma

114 Platelet-poor plasma was generated from healthy volunteers (N=4), patients presenting with
115 MI (N=6) and from the same patients 1-month post-MI. 10-20 mL of whole blood was
116 collected in EDTA (Greiner Bio-One, Stonehouse, United Kingdom) coated tubes and
117 centrifuged at 1,000 x g for 25 minutes. The plasma was collected and centrifuged again for
118 10 minutes at 5,000 x g to produce platelet-poor plasma. The platelet-poor plasma was
119 stored in 500 μ L aliquots at -80 °C for future use.

120

121 Isolation of plasma EV using UC

122 Plasma aliquots were thawed at room temperature and EV were isolated by UC by
123 transferring 500 μ L of platelet-poor plasma from healthy volunteers or 100 μ L from platelet-
124 poor plasma from MI patients to a 13.2 mL QuickSeal tube (Beckman Coulter, California,
125 United States). The tubes were filled with a 16 G hypodermic needles (Microlance, VWR,
126 Pennsylvania, United States) fitted to a 10 mL syringe (VWR, Pennsylvania, United States)
127 and after plasma was injected into the tube, 13 mL of phosphate buffered saline (PBS,
128 Thermo Fischer Scientific, Massachusetts, United States) was added. The tubes were
129 sealed using a soldering iron (Zacro, 60 W) and centrifuged using an Optima MAX-XP
130 ultracentrifuge (Beckman Coulter, California, United States) at 120,000 x g for 120 minutes
131 at 4 °C with a MLA55 fixed-angle rotor (Beckman Coulter, California, United States) [5, 6].
132 The pelleted plasma EV were resuspended in 100 μ L PBS or RIPA buffer (Thermo Fischer
133 Scientific, Massachusetts, United States) for subsequent analysis.

134

135 Isolation of plasma EV using precipitation

136 Plasma EV were isolated by precipitation by using the Total Exosome Isolation Kit
137 (Invitrogen, Massachusetts, United States). 500 μ L of platelet-poor plasma from healthy
138 volunteers or 100 μ L of platelet-poor plasma from MI patients was thawed at room
139 temperature. After vortexing, 20-100 μ L of the Exosome Precipitation Reagent (Total
140 Exosome Isolation Kit (for plasma), ThermoFisher Scientific, Massachusetts, United States)
141 was added and mixed by repeated pipetting. Samples were incubated for 30 minutes on ice,
142 the mixture was centrifuged at 10,000 \times g for 10 minutes by a Heraeus Fresco 17 benchtop
143 centrifuge (ThermoFisher Scientific, *ibid*) at room temperature. The supernatant was
144 removed and samples were centrifuged again at 2,000 \times g for 2 minutes to remove residual
145 supernatant. The pelleted plasma EV were resuspended in 100 μ L PBS or RIPA buffer for
146 downstream analysis by repeated pipetting.

147

148 Isolation of plasma EV using acoustic trapping

149 Acoustic trapping of plasma for the isolation of EV was achieved by diluting plasma 1:1 with
150 PBS as previously described [18]. Briefly, samples were loaded onto a Costar 96-well plate
151 (Corning, New York, United States) and inserted in the AcouSort device (Version 2.0)
152 (AcouSort AB, Lund, Sweden). Acoustic waves were produced by a waveform generator
153 (Keysight 33210A, Keysight, California, United States) with a 9.2 V output and were directed
154 into a borosilicate capillary acoustic trapping unit (AcouSort AB, Lund, Sweden). Following
155 activation of the waveform generator and the acoustic trapping unit was initialised, 50 μ L of
156 12 μ m polystyrene beads (AcouSort AB, Lund, Sweden) were loaded into the acoustic
157 trapping unit using a syringe pump (Tricontinent C2400 (Tricontinent, Fürstfeldbruck,
158 Germany) set to 50 μ L/min. Each run consisted of 100 μ L of 1:1 diluted plasma and were
159 loaded with a syringe pump speed of 20 μ L/min. After acoustic trapping, the samples were
160 washed by aspirating 15 μ L of PBS at 20 μ L/min and dispensing 50 μ L at 20 μ L/min. After
161 the PBS wash, the samples were eluted in 50 μ L of PBS and used for downstream analysis.

162

163 Isolation of plasma EV using size exclusion chromatography

164 Size exclusion chromatography (SEC) isolation of plasma EV was achieved by using the
165 Exo-spin™ 96 (Cell Guidance Systems, Missouri, United States) [27]. Columns were
166 equilibrated at room temperature for 15 minutes prior use. Afterwards, the columns were
167 washed twice with 250 µL of PBS. Plasma was thawed at room temperature and 100 µL of
168 plasma from healthy volunteers or MI patients was loaded into each column. Plasma EV
169 were eluted by adding 200 µL of PBS to the top of the column eluted under gravity. Plasma
170 EV were collected and stored for subsequent analysis.

171

172 Isolation of plasma EV using immunoaffinity capture

173 Prior to isolation, the plasma was passed through a SEC method as described above.
174 Exosome-Human CD9 Isolation Reagent, Exosome-Human CD63 Isolation/Detection
175 Reagent and Exosome-Human CD81 Isolation Reagent (all Invitrogen, Massachusetts,
176 United States) were used to capture plasma EV. The mixture was created by resuspending
177 each bead solution and mixing by repeated pipetting. Control IgG-isotype (10400C, Thermo
178 Fischer Scientific, Massachusetts, United States) matched beads were conjugated according
179 to the instructions of the Dynabeads Antibody Coupling Kit (Invitrogen, Massachusetts,
180 United States). After SEC pre-isolation, the samples were incubated with 80 µL of the
181 combined CD9, CD63 and CD81 beads (end concentration 1×10^7 / mL, equal quantity of
182 each bead mixture) or equally concentrated IgG control beads at 4 °C for 18 hours under
183 continual rotation by a vertical rotor (Grant Bio, Essex, United Kingdom). After incubation,
184 the beads were pelleted for 5 minutes at room temperature using a Dynal Magnet
185 (Invitrogen, Massachusetts, United States) and the supernatant was collected for
186 subsequent analysis. Following pelleting, the samples were washed three times with 200 µL
187 of PBS and magnetic beads were pelleted as described above. Following the washes, the
188 beads were resuspended in RIPA buffer and supernatant was separated by using a 2,000 x
189 g spin and collected for subsequent analysis.

190

191

192 Nanoparticle Tracking Analysis

193 Plasma EV size distribution and concentration were determined by Nanoparticle Tracking
194 Analysis (NTA) using a Zetaview device (Particle Metrix, Inning am Ammersee, Germany) as
195 previously described [5, 6]. Prior to injection into the sample chamber, samples were diluted
196 in PBS. The Zetaview measured the sample chamber from 11 positions in 2 cycles. The
197 settings were set at sensitivity 80, fame 30 and shutter speed 100. Silica 100-nm
198 microspheres (Polysciences Inc., Philadelphia, United States) were used to quality check the
199 instrument performance routinely. The particle concentration per method was calculated as
200 the change (Δ) compared to the the control sample, in which PBS replaced the plasma
201 sample.

202

203 Protein concentration

204 Protein concentration was determined by bicinchoninic assay (BCA) (Thermo Fischer
205 Scientific, Massachusetts, United States). A standard curve with Bovine Serum Albumin
206 (Thermo Fischer Scientific, Massachusetts, United States) was used to calculate the protein
207 concentration. Isolated EV were diluted 1:2 or 1:6 with RIPA buffer and needle sonicated by
208 a SonoPuls HD2070 (Bandelin, Berlin, Germany) at 40% power for 10 seconds. 25 μ L of
209 sonicated sample or standard was incubated in duplicate with 175 μ L of a 25:1 ratio between
210 Reagent A and Reagent B (Thermo Fischer Scientific, Massachusetts, United States) and
211 incubated at 37 °C for 30 minutes. After incubation, absorbance was measured at 562 nm
212 using a plate reader (FLUOstar Omega plate reader, BMG Labtech, Aylesbury, United
213 Kingdom).

214

215 Transmission Electron Microscopy

216 Transmission electron microscopy (TEM) of the isolated EV was conducted as previously
217 described [6]. Briefly, grids (300 mesh Cu carbon film) were glow discharged for 20 seconds

218 at 15 mA (Leica EM ACE 200). The isolated plasma EV samples were added to the grid for 2
219 minutes, blotted, stained with 2% uranyl acetate for 20 seconds, blotted and allowed to air
220 dry. Images were acquired on a 120 kV Tecnai 12 TEM (Thermo Fischer Scientific,
221 Massachusetts, United States) equipped with a OneView digital camera (Gatan, California,
222 United States). TEM images of control samples, in which the isolation method was run with
223 PBS in the place of the plasma, were obtained for each method. Immunoaffinity-based
224 isolated EV were fixed with 1.6% glutaraldehyde in PBS for 1 hour at 4 °C. Following
225 fixation, the beads were fixed in 4% agarose with PBS. The agarose was cut into small
226 cubes (1-2 mm³). Sections were collected onto 200 mesh Cu grids and imaged using a
227 Gatan OneView camera with a FEI Tecnai 12 TEM at 120kV.

228

229 Proteomics

230 Isolated plasma EV were processed for proteomics as previously described [28, 29]. In
231 short, the samples were reduced in 5 mM dithiothreitol for 30 minutes at room temperature.
232 Subsequently, the samples were alkylated with 20 mM iodoacetamide for 30 minutes and
233 precipitation using chloroform-methanol precipitation. Quantified protein groups with ≥ 2
234 unique peptides were included in the comparison of proteomes. The LFQ values for each
235 protein group was deducted by the LFQ from control samples per isolation method. Protein
236 abundance was normalised by Log-transformation. Gene Ontology (GO) analysis of the
237 protein groups [30] was conducted by using Genontology.org [30] and the data were
238 extracted on 19-07-2021. P-values were corrected for false discovery rate (FDR) and
239 significance was set at $p < 0.05$. Fisher exact tests were conducted using R on published
240 databases EVpedia [31], Vesiclepedia [32] and Exocarta [33].

241

242 EV-Array

243 Isolated plasma EV were analysed by a targeted EV-Array, which has been described
244 previously [6, 34]. In short, a protein microarray plate was generated with the following
245 antibodies: CD146 (P1H12), Flotillin-1, TSG101 (Abnova, Taiwan), CD9, CD81 (AnCell

246 corporation, Minnesota, United States); CD16 (3G8, BD Biosciences, California, United
247 States); Alix (3A9), VEGFR2 (7D4-6; Biolegend, California, United States); CD63 (Bio-Rad,
248 California, United States); ICAM-1 (R6.5, eBioscience, California, United States); Endoglin
249 (LSbio, Washington, United States); Tissue factor (323,514), VCAM-1 (HAE-2Z),
250 Thrombomodulin (501733), CD31 (AF806, R&D Systems, Minnesota, United States), VE-
251 Cadherin (AF938, R&D Systems, Minnesota, United States). After blocking with the blocking
252 buffer (50 mM ethanolamine, 100 mM Tris, 0.1% SDS, pH 9.0) for 30 minutes, the wells
253 were emptied, and the plate was dried for 5 hours and sealed. The samples were incubated
254 in the antibody coated microarray plate overnight at 2-8 °C. Following a wash, each well was
255 incubated with a 100 µL of a detection antibody cocktail (biotinylated anti-human-CD9, -
256 CD63 and -CD81 (Ansell, Minnesota, United States). After another wash, 100 µL
257 streptavidin-Cy3 Life Technologies, Massachusetts, United States) diluted 1:3,000 was
258 added to each well and incubated for 30 minutes. The plate was scanned using a
259 sciREADER FL2 microarray scanner (Scienion AG, Berlin, Germany), at 535 nm and an
260 exposure time of 2,000 milliseconds. For each protein the control, PBS sample value was
261 subtracted from the result.

262

263 Western blot

264 Isolated plasma EV or controls were lysed using RIPA buffer with protease and phosphatase
265 inhibitors PhosSTOP (Roche, Basel, Switzerland) and cOmplete (Roche, Basel, Switzerland)
266 and were needle sonicated by a SonoPuls HD2070 (Bandelin, Berlin, Germany) at 40%
267 power for 10 seconds as previously described [5, 6]. Following sonication, samples were
268 incubated at 95 °C for 5 minutes to reduce. 8 µg of protein was combined with NuPage LDS
269 sample buffer (4x) agent (Invitrogen, Massachusetts, United States). The samples were
270 loaded onto a 4-12% bis-tris gradient gel (NuPAGE 4-12% Bis-Tris Protein Gel; 1.5 mm
271 (ThermoFisher Scientific, Massachusetts, United States) with Amersham ECL Full Range
272 ladder (Cytiva Life Sciences, Massachusetts, United States). Separated samples were
273 transferred to a nitrocellulose membrane (Amersham Proton 0.2 µm, GE Healthcare, Illinois,

274 United States) and blocked for non-specific binding in 5 % skimmed milk powder (Marvel
275 Original, New York, United States) in 0.5% PBS-tween 20 (Sigma-Aldrich, Missouri, United
276 States) for 1 hour. Membranes were incubated with primary antibodies overnight: ALIX
277 (ab117600, Abcam, Cambridge, United Kingdom) (1/1,000 dilution), CD63 (EXOAB-KIT-1,
278 System Biosciences, California, United States) (1/1,000 dilution), ApoB (Ab139401, Abcam,
279 Cambridge, United Kingdom) (1/20,000 dilution), albumin (MAB1455, R&D Systems,
280 Minneapolis, Canada) (1/8,000 dilution), ApoA-I (Mab36641, R&D systems, Minneapolis,
281 Canada) (1/8,000 dilution) and H3 (D1H2, Cell Signalling Technology, Massachusetts,
282 United States) (1/1,000 dilution) 5 % milk in PBS-tween (PBS-T). Membranes were washed
283 three times with PBS-T and incubated with secondary-horse radish peroxidase (HRP)
284 conjugated antibodies (1/20,000 α -mouse W402B or 1/50,000 α -rabbit W401B, Promega,
285 Wisconsin, United States) for 1 hour. The membranes were washed once again with PBS-T
286 before incubating them with enhance chemiluminescence substrate (Pierce ECL,
287 ThermoFisher Scientific, Massachusetts, United States) for imaging (Bio-Rad ChemiDoc MP
288 Imaging system, California, United States).

289

290 Sphingolipidomics

291 Sphingolipids were determined as previously described [35]. 25 μ L of each sample were
292 combined with 10 μ L solution containing labelled sphingolipid internal standards in LC-MS
293 Methanol (Honeywell, North Carolina, United States) was added to each sample. This was
294 followed by the addition of 100 μ L of methanol to each sample. Samples were then vortexed
295 for 30 seconds and sonicated for 15 minutes in a Fisherbrand Ultrasound bath S60 (Fischer-
296 Scientific, Massachusetts, United States) with ice. Next, samples were centrifuged at 12,000
297 x g during 15 minutes at 6°C. Finally, 80 μ L of the supernatant were transferred to an LC-
298 MS amber vial (Waters, Wilmslow, United Kingdom) equipped with a 150 μ L insert. Samples
299 were randomized by time point of the individual within an extraction method. Samples were
300 analyzed on an Acquity UPLC coupled to a Xevo TQ-S Mass Spectrometer (Waters,
301 Wilmslow, United Kingdom) as previously described.

302

303 Bioinformatics and Integrated analysis

304 Integrated analysis was conducted by combining data from the NTA, protein concentration,
305 EV-Array, proteomic and sphingolipidomic analysis. The data was normalized per row and
306 log transformed. Following data normalization, a principal component analysis was
307 conducted in R 4.0.0 [37] using the *factoextra* [38] and *FactoMineR* [39] packages. For
308 visualization *ggplot2* [40] was used. Each of the principal components were then used to
309 create a heatmap by extracting the values from the eigenvalues for each of the principal
310 components and processing them in *pheatmap* [41]. The data was clustered by using double
311 hierarchical clustering using the *pheatmap* R package.

312

313 Data availability

314 All data produced in the present study are available upon reasonable request to the
315 Corresponding Author.

316

317 Statistical analysis

318 Data was plotted as mean with standard deviation. Normality of the data was confirmed
319 using QQ plot and D'Agostino-Pearson normality test. For paired analysis, at the two time
320 points, or for two independent groups, paired or unpaired Students T-test were used
321 respectively (GraphPad Prism 9). Correlation analysis was carried out using linear Pearson
322 regression analysis (Graphpad Prism 9). One-way ANOVA with Bonferroni correction post-
323 hoc tests were used for analyses with >3 independent groups. The proteomic and lipidomic
324 data was analyzed using a Kruskal-Wallis statistical test with Bonferroni post-hoc tests. p
325 values <0.05 were considered significant.

326 **Results**

327 Plasma EV number and size is influenced by the isolation method

328 The concentration of isolated EV (expressed as delta over a matched PBS or and IgG
329 control sample) determined by NTA differed per method (UC $9.5 \times 10^9 \pm 1.8 \times 10^9$ EV / mL,
330 precipitation $6.1 \times 10^{11} \pm 2.7 \times 10^{11}$ EV / mL, acoustic trapping $6.4 \times 10^9 \pm 2.8 \times 10^9$ EV / mL,
331 SEC $5.5 \times 10^9 \pm 1.9 \times 10^9$ EV / mL and immunoaffinity $2.8 \times 10^{10} \pm 7.1 \times 10^9$ EV / mL, **Figure**
332 **2A**). In agreement with previously published studies, precipitation yielded significantly higher
333 numbers of particles / mL compared to UC [15, 36] and SEC [15, 37] (both $p < 0.01$). Plasma
334 EV number, isolated by precipitation, were also higher than the concentration acquired by
335 acoustic trapping or by immunoaffinity capture (both $p < 0.01$) (**Figure 2A**). The size and
336 concentration distribution for each biological replicate exhibited uniformity within each
337 isolation method and the different isolation methods did give a similar size distribution profile
338 overall, which ranged from 15 nm (**Figure 2B**). However, the mean size of EV isolated by
339 UC was significantly higher compared to the other methods (UC 143.7 ± 3.4 nm, versus
340 precipitation 94.2 ± 3.9 nm, acoustic trapping 81.2 ± 3.9 and SEC 87.2 ± 1.5 , $p < 0.01$ all)
341 (**Table 1**).

342

343 Plasma EV protein concentration

344 The protein concentration (expressed as the change over a matched PBS or and IgG
345 control) also differed across the EV isolation methods: UC 982 ± 113 μg / mL, precipitation
346 $9,478 \pm 3,174$ μg / mL, acoustic trapping $1,211 \pm 141$ μg / mL, SEC 382 ± 51 μg / mL and
347 immunoaffinity 33 ± 12 μg / mL (**Figure 2C**). EV generated by precipitation had a
348 significantly higher protein concentration compared to UC, acoustic trapping, SEC or
349 immunoaffinity (all $p < 0.01$, **Figure 2C**). The purity of EV isolation can be estimated by
350 calculating a ratio of EV number (EV / mL) to protein concentration (μg / mL) [44]. The EV
351 purity ratio differed between isolation method: UC $9.0 \times 10^6 \pm 1.4 \times 10^6$; precipitation $4.7 \times$
352 $10^8 \pm 1.5 \times 10^8$; acoustic trapping $2.1 \times 10^7 \pm 7.6 \times 10^6$; SEC $6.8 \times 10^6 \pm 4.0 \times 10^6$ and
353 immunoaffinity capture $3.1 \times 10^8 \pm 1.0 \times 10^8$. Both the immunoaffinity and precipitation

354 methods achieved a significantly higher EV purity ratio when compared to UC, SEC or
355 acoustic trapping ($p < 0.01$ compared to all methods) (**Supplemental Figure 1**).

356

357 Plasma EV protein characterisation by Western blot

358 As NTA is unable to distinguish between plasma EV and similarly sized protein aggregates
359 and lipoproteins, we analysed the isolated plasma EV obtained from each method for a
360 number of markers by western blotting. ALIX and CD63 were included as the EV markers.
361 For the plasma lipoprotein contaminants, we measured ApoB and ApoA-I. Histone H3 for
362 cellular contaminant by western blot and albumin was also included in the set. Each isolation
363 method showed the presence of EV markers ALIX and CD63 (**Figure 2D**). Apolipoproteins
364 (ApoA-I and ApoB) were also present in all isolation methods. All methods were negative for
365 markers of cellular contamination by histone H3. Surprisingly, the IgG isotype control for
366 immunoaffinity capture using CD9, CD63 and CD81 also showed the presence of EV
367 markers ALIX, CD63 and ApoB, albumin, ApoA-I but histone H3 was absent (**Figure 2D**).

368

369 Plasma EV morphology by TEM

370 To determine the morphology of isolated plasma EV, we undertook TEM for the five different
371 plasma EV isolation methods versus a matched PBS control or an IgG control for
372 immunoaffinity capture beads. TEM analysis showed EV-like particles for each isolation
373 method and an absence of EV-like particles in their respective PBS isolation controls
374 (**Figure 2E-H**). Immunoaffinity beads CD9, CD63 and CD81 were embedded in agar and
375 sectioned to visualise the bead surface for EV-like structures versus the IgG control. IgG
376 control showed no EV-like particles present (**Figure 2I**). Immunoaffinity capture using CD9,
377 CD63 and CD81 beads showed intact EV-like particles captured on the bead surface
378 (**Figure 2J**).

379

380 Plasma EV compositional analysis using a high throughput protein EV-Array

381 The results detailed above provide evidence for the relative success of each method to yield
382 plasma EV and assessment of relative plasma EV purity [39]. However, these techniques do
383 not readily distinguish the abundance of specific plasma EV populations carrying, for
384 instance, specific cell-associated markers, or easily allow quantitative assessment of the
385 abundance of contaminating lipoproteins. Thus, we probed the composition of the plasma
386 EV isolated from each method for general EV markers CD9, CD63, CD81, ALIX, TSG101,
387 Flotillin 1, Annexin V and a panel of 18 cell associated markers, which may distinguishes EV
388 from platelets, endothelial cells, immune cells, muscle and lipoprotein contaminants
389 apolipoprotein E (ApoE) and apolipoprotein H (ApoH) using a validated high throughput EV-
390 protein antibody array (**Figure 3**) [34]. We utilised a matched PBS control for UC,
391 precipitation, acoustic trapping and SEC and an IgG control for immunoaffinity capture. For
392 the EV-associated proteins, CD9 and CD81, they were significantly higher in plasma EV
393 isolated by UC compared to the other methods ($p < 0.01$ for both). Annexin V was significantly
394 higher in the acoustic trapping samples compared to SEC and immunoaffinity capture
395 ($p < 0.01$ and $p < 0.05$, respectively).

396

397 Hierarchical clustering of the EV-Array acquired data for the different isolation methods
398 indicates that there are significant method-dependent differences for cell associated EV
399 markers (**Figure 3**). CD31 was significantly higher in precipitation isolated plasma EV versus
400 acoustic trapping ($p < 0.05$). CD41 was significantly higher in UC isolated plasma EV
401 compared to precipitation isolated EV ($p < 0.05$) and CD16 content was significantly higher in
402 the precipitation isolated plasma EV samples compared to SEC ($p < 0.01$). There were no
403 differences between immunoaffinity capture using CD9, CD63 and CD81 and IgG controls
404 (**Figure 3**).

405

406

407 Unbiased proteomic analysis of plasma EV

408 We next determined the proteomic profile of each isolation method using unbiased LC-
409 MS/MS versus their respective PBS or IgG controls for each method. The proteomic profile
410 following plasma EV isolation showed a significantly higher number of quantified protein
411 groups compared to their respective controls for all isolation methods, except immunoaffinity
412 capture, which displayed similar results to the IgG control beads (UC $p < 0.01$, precipitation
413 $p < 0.05$, acoustic trapping $p < 0.01$ and SEC $p < 0.01$, **Figure 4A**). The choice of plasma EV
414 isolation method influenced the overall EV-proteome, but nine protein groups were common
415 across all methods (**Supplemental Figure 2**). These were: immunoglobulin heavy constant
416 gamma 1, alpha-2-macroglobulin, haptoglobin, immunoglobulin heavy constant μ ,
417 immunoglobulin kappa constant, serpin family A member 1, albumin, fibrinogen alpha chain
418 and Apo-A1.

419

420 We used hierarchical clustering of the top 30 quantified protein groups across the different
421 plasma EV isolation methods and found a distinct separation between isolation methods. UC
422 and SEC isolated plasma EV clustered together and precipitation, acoustic trapping and
423 immunoaffinity capture formed a distinct separate cluster (**Figure 4B**). Hierarchical clustering
424 indicates that these differences between UC/SEC and precipitation, acoustic trapping and
425 immunoaffinity capture were driven by an abundance of protein groups with common plasma
426 proteins (ALB, A2M, ApoB, C3, TF, HP, Apo-A1, SERPINA1, CP and ITIH2), fibrinogens
427 (FGG and FGB) and immunoglobulins (IGHG1, IGKC, IGHG3, IGHM, IGK, IGHG2).

428

429 To better understand the nature of the proteomic profile for each isolation method, we
430 conducted unbiased Gene Ontology (GO) pathway analysis of the protein groups associated
431 with each isolation method. All methods showed a significant association with EV pathways:
432 Blood Microparticle GO: 0072562 and Extracellular Exosome GO:0070062 (all $p < 0.01$,
433 **Supplemental Figure 3A**). However, there was no clear separation between the different
434 isolation methods using this pathway analysis approach. To further scrutinize the EV
435 proteomic profile obtained per plasma EV isolation method we undertook a statistical

436 comparison using a Fisher's exact test with published EV-databases EVpedia [31],
437 Vesiclepedia [32] and Exocarta [33]. This determined the similarity between plasma EV
438 proteomic profiles obtained from the five different isolation methods to those published
439 previously by showing the size of the intersect. There was a significant overlap between the
440 five different isolation methods and the archived EV databases ($p < 0.05$, all methods,
441 **Supplemental Figure 3B**). UC, SEC and immunoaffinity capture showed the greatest
442 similarity with published databases. Whereas precipitation and acoustic trapping showed
443 less similarity. Furthermore, we determined whether our plasma EV acquired proteomic
444 profiles from the five different methods were similar to previously published plasma EV
445 proteomic data for Exospin, SEC, ExoQuick, IZON35, IZON70, Optiprep and Exo-easy [16,
446 17] and found a significant overlap for all five plasma EV isolation methods ($p < 0.01$)
447 **(Supplemental Figure 4)**.

448

449 Targeted sphingolipidomic of plasma EV

450 EV membranes are largely composed of lipids [46] and lipoproteins are a predominant
451 contaminant in plasma EV samples [41], which are influenced by the choice of isolation
452 method [12, 42]. We compared the lipidomic profile of the different plasma EV isolations
453 methods by undertaking targeted sphingolipidomic analysis. The sphingolipidomic analysis
454 showed a significantly higher number of sphingolipids compared to the respective controls
455 for all isolation methods except immunoaffinity capture (UC $p < 0.01$, precipitation $p < 0.05$,
456 acoustic trapping $p < 0.01$ and SEC $p < 0.01$, **Figure 5A**). However, there were distinct
457 sphingolipidomic differences between the other methods. Eleven of the quantified
458 sphingolipids were common to all methods, which were DhCer(d18:0/24:0), Cer(d18:1/22:0),
459 Cer(d18:1/24:1), Cer(d18:1/24_:0), SM(d18:1/16:0), SM(d18:1/18:0), SM(d18:1/24:1),
460 SM(d18:1/24:0), HexCer(d18:1/16:0), HexCer(d18:1/24:1) and LacCer(d18:1/24:1)
461 **(Supplemental Figure 5)**. Hierarchical clustering analysis of the sphingolipidomic profile for
462 each of the isolation methods showed that there are three distinct clusters **(Figure 5B)**.
463 Immunoaffinity capture and precipitation formed two separate individual clusters, whilst UC,

464 acoustic trapping and SEC clustered together. Hierarchical clustering indicates that these
465 group differences were driven by an abundance of sphingomyelins (16:0, 18:0, 24:0 and
466 24:1), ceramides (22:0, 24:0 and 24:1), hexosylceramides (24:1) and lactosylceramides
467 (16:0) in the precipitation group and a lack of these sphingolipids in the immunoaffinity
468 capture group.

469

470 Integrated comparison of plasma EV isolation methods

471 These data shows that plasma EV isolation methods have divergent impact on the yield of
472 EV, their purity, the type of EV isolated from plasma that are associated with a particular cell
473 source and the overall proteomic and sphingolipidomic profile. To better understand how
474 these individual method associated differences influenced the plasma profile, we undertook
475 integrated analysis of all the different plasma EV isolation methods with all of the acquired
476 data. This included the EV particle concentration, protein concentration, EV-protein array
477 data, proteomic and sphingolipidomic data. To condense the multiple different variables, we
478 converted the data into principal components. Principal component analysis with two
479 components (PCA1 and PCA2) accounted for 47.2% of the variance and showed clear
480 separation between the different isolation methods (**Figure 6A/B**). UC, SEC and
481 precipitation form distinct clusters, whereas acoustic trapping and immunoaffinity capture
482 clustered together. Specific principal component analysis indicated that the PCA1 is driven
483 by proteomics acquired data and PCA2 is driven by sphingolipidomic data (**Supplementary**
484 **Figure 6**). These integrated data show that the EV isolation method influences the omic and
485 integrated-based plasma EV-profile, which may influence interpretation of EV-acquired data
486 for clinical biomarker discovery and precision diagnostics.

487

488 Plasma EV isolation methods influence the diagnostic potential of plasma EV from patients 489 following MI

490 We next determined whether the choice of plasma EV isolation method impacts the ability to
491 detect changes in EV-profile in a disease state. We obtained plasma at time of presentation

492 with MI, but prior to percutaneous coronary intervention (PCI), and a matched control plasma
493 sample was obtained at 1-month post-MI from the same patients. The clinical patient
494 characteristics are detailed in **Table 2**.

495

496

497

498 Plasma EV concentration in MI is influenced by the isolation method

499 To mitigate any potential variability in bio-banked plasma samples we used three technical
500 plasma replicates per patient, per time point and per method. There were significantly more
501 plasma EV at time of presentation with MI versus the 1 month control follow up when plasma
502 EV were isolated by UC, precipitation and acoustic trapping ($p < 0.05$ for all) (**Figure 7A**), but
503 not by SEC and immunoaffinity capture (UC presentation: 2.8×10^9 EV / mL vs. UC follow-
504 up: 2.1×10^9 EV / mL; precipitation presentation: 1.5×10^{12} EV / mL vs. precipitation follow-
505 up: 7.9×10^{11} EV / mL; acoustic trapping presentation: 4.3×10^{10} EV / mL vs. acoustic
506 trapping follow-up: 1.9×10^{10} EV / mL; SEC presentation: 2.5×10^{11} EV / mL vs. SEC follow-
507 up: 9.2×10^{10} EV / mL and immunoaffinity presentation: 2.0×10^{11} EV / mL vs.
508 immunoaffinity capture follow-up: 9.8×10^{10} EV / mL, **Figure 7A**). The technical variance
509 between the three independent isolations from each patient, and at each time, point showed
510 that SEC gave significantly less variance compared to UC (10.0 ± 3.1 % vs. 22.7 ± 13.0 %, $p < 0.01$) (**Supplemental Figure 7A**). The mean plasma EV size was similar between the
511 time of presentation and 1 month follow up control for the five different plasma EV isolation
512 methods (**Supplemental Figure 7B**) and the size and concentration distribution profile
513 showed no distinct differences between time points or dependent on the plasma EV isolation
514 method (**Supplemental Figure 7C**).

515

516
517 The plasma EV isolation method influences plasma EV concentration association with infarct
518 size

519 We have previously reported that the total concentration of plasma EV in the peripheral
520 blood isolated by UC at the time of presentation correlates with the size of myocardial injury
521 and scar, determined by late gadolinium enhanced (LGE) MRI 6 months post-MI [5, 6].
522 Therefore, we determined whether plasma EV concentrations from the five different plasma
523 EV isolation methods influenced the ability to determine this important clinical association.
524 Infarct size at 6-months post-MI significantly correlated with the plasma EV concentration at
525 time of presentation for UC samples ($R^2 = 0.89$, $p=0.02$), but not for precipitation, acoustic
526 trapping, SEC or immunoaffinity capture ($R^2=0.10$ $p=0.60$, $R^2=0.16$ $p=0.50$, $R^2=0.05$ $p=0.71$
527 and $R^2=0.10$, $p=0.78$, respectively) (**Figure 7B**).

528

529 Cell associated plasma EV are not influenced by the isolation method in MI

530 We determined whether the isolation methods influenced cell associated plasma EV-
531 markers in MI patients at presentation versus the respective 1 month follow up sample. The
532 high through put EV-Array data was expressed as fold change over the matched follow-up
533 control samples per patient. Plasma EV markers were increased at time of presentation vs.
534 follow-up control (**Figure 7C**). However, the pattern of change in plasma EV-markers were
535 not consistent across the different isolation methods (**Figure 7C**). Hierarchical clustering of
536 the plasma EV marker response at the time of presentation with MI showed method-
537 dependent clustering. Similarly, cell associated markers on plasma EV were differentially
538 enriched following MI (**Figure 7C**). Once again, unbiased clustering showed method-
539 dependent groupings. Together these data suggest that changes in plasma-EV protein are
540 influenced by the choice of plasma EV isolation method following MI in isolation and when
541 clustered together.

542

543 Plasma EV sphingolipidomic profiles are altered following MI and influenced by the isolation 544 method

545 Next, we profiled EV-sphingolipids in the acute phase following MI (calculated as fold over
546 matched follow-up control samples) using the different plasma EV isolation methods. Plasma

547 EV-sphingolipidomic profiles for samples generated by precipitation, acoustic trapping and
548 SEC contained significantly more quantified lipid groups at time of presentation with MI
549 versus samples obtained by UC and immunoaffinity capture ($p < 0.01$, all). We ranked plasma
550 EV-lipid profiles based on their overall abundance of lipid groups and found that ceramides
551 were significantly higher in the precipitation isolated plasma EV samples, followed by SEC,
552 acoustic trapping, ultracentrifugation / immunoaffinity capture ($p < 0.01$). Whereas the
553 sphingomyelins were significantly higher in the precipitation group versus all other isolation
554 methods ($p < 0.001$) (**Figure 7D**). The clustered plasma EV-sphingolipid profile following MI
555 was influenced by the choice of isolation method. Several ceramides and sphingomyelins
556 were significantly higher in the plasma EV isolated by precipitation or acoustic trapping
557 compared to UC (**Supplemental Figure 8**). In addition, the fold increase of Cer(d18:1/22:0),
558 SM(d18:1/18:1) and sphinganine (d18:0) in plasma EV isolated by precipitation at time of
559 presentation vs. 1-month follow up significantly correlated with the infarct size of the patients
560 at 6-months post-MI ($R^2 = 0.91$ $p = 0.01$, $R^2 = 0.78$ $p = 0.05$ and $R^2 = 0.78$ $p = 0.05$, respectively)
561 (**Supplemental Figure 9**). This result further confirmed that plasma EV isolation methods,
562 using targeted sphingolipidomic methods, are associated with unique method dependent
563 profiles in patients following MI.

564

565 Integrated-omics comparison of plasma EV isolation methods in MI patients

566 Finally, we integrated all the acquired plasma EV data from the MI patients in the acute
567 presentation and follow-up time points. A principal component analysis was constructed to
568 assess if the plasma EV profile at time of presentation differed from follow-up using a 95%
569 confidence level. Integrated analysis showed that plasma EV profiles were only
570 distinguishable at time of presentation with MI for precipitation and acoustic trapping, but not
571 for those plasma EV isolated by UC, SEC and immunoaffinity capture (**Figure 8**). These
572 findings indicate that different plasma EV isolation methods influence the diagnostic potential
573 of plasma liberated EV following MI when multiple datasets are integrated to determine
574 plasma EV profiles for potential panel biomarker discovery.

575 **Discussion**

576 Plasma EV-cargo may provide unparalleled insight into tissue homeostasis and pathological
577 processes to facilitate identification of patients for focused therapies, but the methods to
578 isolate plasma EV may impact the EV characteristics. Here, we found that; (I) the choice of
579 plasma EV isolation method affected the plasma EV concentration, sphingolipid and
580 proteomic profile, (II) but the five different plasma EV isolation methods shared a common
581 EV protein and sphingolipid profile. (III) Plasma EV isolation by immunoaffinity capture using
582 anti-CD9, -CD63 and -CD81 coated antibody beads with the current protocol yields a similar
583 profile to IgG control beads. (IV) The isolation method affected the ability to detect
584 alterations in plasma EV sphingolipids and proteins in MI patients and (V) their association
585 with infarct size determined by cardiac MRI 6 months post-MI. For example, the plasma EV
586 concentration at time of presentation obtained using UC provides prognostic information, but
587 this method is less suitable as a tool to generate EV with higher purity for use in mechanistic
588 studies.

589

590 Previous studies have sought to determine the influence of plasma EV isolation methods,
591 but have often focused on comparing the net influence on the EV-proteome [3, 16, 17, 43] or
592 RNA profiles [16] after isolation. These approaches can neglect the increased dimensionality
593 of EV components, which carry numerous biologically active molecules such as proteins,
594 lipids, RNA/DNA and metabolites. Furthermore, there is varied assessment of
595 contaminations in EV preparations for use in 'omics' studies, which may mask or skew the
596 interpretation of datasets. The approach employed here utilizes the same independent
597 biological replicates across multiple methods for plasma EV isolation and characterization, in
598 conjunction with a control PBS/vehicle sample or an IgG for immunoaffinity capture beads.
599 Here, the repeated analysis of the same plasma samples across multiple methods has
600 enabled individual biological variability and potential plasma EV isolation irregularities to be
601 explored. By using individual and integrated analysis, we showed that each method of
602 plasma EV isolation was internally consistent; in so much that the samples clustered

603 according to their isolation method in unsupervised hierarchical clustering and principal
604 component analysis of all the acquired data.

605

606 Consistent with previous reports, our plasma EV-proteome was dependent on the plasma
607 EV isolation method [16, 17]. However, our data shows that there are common plasma
608 proteins, such as albumin and apolipoproteins ApoA-I and ApoB, present in all five isolation
609 methods tested, with significant similarities to archived EV-databases [31-33] and published
610 studies [16, 17, 31]. In particular, the plasma EV-proteome indicated that UC/SEC cluster
611 together based on the top 30 protein groups quantified, due to higher quantities of
612 fibrinogens and immunoglobulins compared to the other methods. This is, potentially, a
613 methodological constraint of employing untargeted mass spectrometry on plasma EV, which
614 favors the most abundant peptides.

615

616 To better determine the protein profile of known plasma EV markers and cell associated
617 markers, we utilized a high throughput EV-Array [50] following plasma EV isolation from the
618 five different methods. We found that CD9 and CD81 were the most abundant in plasma EV
619 derived by UC versus precipitation and SEC in healthy volunteers. Additionally, we found
620 that cell-associated markers such as CD41 (platelets) and CD16 (immune cells) were
621 enriched in UC and precipitation compared to other methods only in healthy volunteers. This
622 high throughput antibody EV-Array circumvents issues of non-EV associated protein and
623 lipid contaminants in plasma EV preparations. However, the five different plasma EV
624 isolation methods used here may have influenced the EV-protein corona. Proteins such as
625 albumin and apolipoproteins (ApoA-I, ApoB, ApoC-III and ApoE) show an association with
626 the surface of EV [45], which may influence antibody mediated binding to the array or
627 subsequent detection of EV-associated proteins in this sandwich ELISA like technique.
628 Protein coronas found on EV are affected by the isolation method [45] and our data shows
629 that the plasma EV-proteome and EV-Array acquired data are also influenced by the
630 isolation method. Indeed, our western blot and proteomic data reported considerable

631 variation in the amount of albumin across the methods, which is a predominant protein in the
632 EV protein corona. In particular, precipitation isolated preparations was associated with
633 lower albumin, which could be due to the presence of PEG and high salt concentrations in
634 the isolation buffer that might be expected to influence albumin associations with the EV
635 protein corona. The temporal dynamics of the EV-protein and possibly EV-lipid corona are
636 poorly understood, and further elucidation of these interactions will be essential to
637 understand the data from these preparations.

638

639 Immunoaffinity based methods, such as magnetic and polystyrene bead conjugations to
640 specific antibodies, such as tetraspanins (CD9, CD63 and CD81), have been heralded as an
641 important advancement in the capture of highly pure EV populations from the plasma.
642 Immunoaffinity based methods could circumvent issues of lipoprotein and protein
643 contamination in plasma EV yields, which are common in methods that use EV physical
644 characteristics such as size and density for isolation such as UC and SEC [16, 46]. To the
645 best of our knowledge this is the first study to compare magnetic beads coated with
646 antibodies for tetraspanins (CD9, CD63 and CD81) with a matched IgG control for plasma
647 EV isolation, using detailed integrated analyses. The plasma EV-profile of proteins and lipids
648 for the immunoaffinity beads and matched IgG control was similar by Western blot, EV-
649 protein-array, the number of peptides groups in proteomic profiles, GO pathway analysis and
650 targeted sphingolipidomics. TEM imaging of IgG beads showed no visible EV-like particles
651 or membranous structures, indicative of whole or sheared EV-particles, captured to the bead
652 surface. However, we hypothesize that soluble non-EV-associated proteins (such as C3,
653 A2M, ALB and fibrinogens A and B) and lipids (such as ApoB, ApoE and ApoA-I) are
654 interacting with IgG beads, which have become associated with EV-profiles in omics studies
655 and in archived databases [31-33]. Studies using less complicated matrices, like conditioned
656 cell culture media, show a more robust distinction between anti-CD9, CD63 and CD81 beads
657 versus IgG control beads [8, 47], indicating that the similarity between tetraspanin and IgG
658 antibody beads here might be matrix specific. Future plasma EV studies using antibody-

659 bead isolation should include a matched IgG control per characterisation when using omic-
660 approaches

661

662 Having determined plasma EV isolations method similarities and differences on the EV-
663 characteristics and cargo in healthy volunteers, we assessed the influence of plasma EV
664 isolation methods in a clinical situation where plasma EV number and composition are
665 altered. We have previously shown that plasma EV are altered following MI to mediate long
666 range signalling and induce the mobilization of splenic-neutrophils, splenic-monocytes and
667 orchestrate their transcriptional programming [5, 6]. The choice of plasma EV isolation
668 method determined whether there was a higher concentration of EV immediately following
669 MI compared to a 1-month follow-up control sample from the same patients. The new data
670 here support our previous observations that the concentration of plasma EV isolated by UC
671 from the time of presentation with MI correlates with the infarct size [5]. However, plasma EV
672 concentrations derived from the other isolation methods in the same patients did not
673 associate with infarct size. One possible explanation is the modest sample size utilised in
674 this multi-method comparison (N=6), which is smaller than those utilised by us in previous
675 publications (N=15-22) [5, 6].

676

677 Plasma EV sphingolipids are predictive of MI [3]. However, the influence of plasma EV
678 isolation methods on the plasma EV-sphingolipidomic profile were not reported. We found a
679 distinct sphingolipid profile between the plasma EV isolation methods. Precipitation-based
680 EV isolation yields a significantly higher lipid content, principally due to higher proportions of
681 sphingomyelins and ceramides. Sphingomyelins are found in cell membranes and
682 associated with high- and low-density lipoproteins [48, 49]. The high presence of
683 sphingomyelins and ceramide in the plasma EV profile of the precipitation-based method is
684 likely due to the co-isolation of lipoproteins. PEG-based solutions co-isolate lipoproteins [56].
685 Lipoproteins contain ApoA-I and ApoB, which were higher in plasma EV derived by
686 precipitation-based isolation when compared to the other methods by Western blot.

687 Lipoproteins can also masquerade as EV-like particles in dynamic light scattering in
688 techniques such as NTA [12]. Precipitation isolated plasma EV had the highest
689 concentration of particles / mL when compared to other methods. EV Cer(d18:1/20:0) only
690 showed elevation in precipitation-based isolation compared other methods. Similarly,
691 precipitation isolated EV showed sphinganine(d18:0) correlated with infarct size at 6-months,
692 but this was not the case for the other methods. Analysis of plasma EV-sphingolipid remains
693 challenging due to constraints due to lipoparticle remnants [57]; however we show here for
694 the first time there are common sphingolipids for different plasma EV isolation methods. In
695 particular, plasma EV-protein and EV-sphingolipids clustered uniquely based on the isolation
696 method, which may impact plasma EV diagnostics where a panel of proteins and
697 sphingolipids are used for differentiation of clinical disease or outcome.

698

699 In summary, our data show that the choice of plasma EV isolation method influences the
700 concentration of plasma EV, the EV-proteome and EV-sphingolipid profile in healthy
701 volunteers and MI patients, where methodological differences determined associations with
702 infarct size. Precipitation based plasma EV isolation gives the highest particle concentration
703 and enriches for more sphingolipids, but co-isolate large quantities of apolipoproteins. In
704 addition, immunoaffinity capture by using antibodies against tetraspanins yields similar EV-
705 protein and EV-sphingolipid profiles to IgG control beads. Unbiased integrated analysis
706 shows that plasma EV isolation methods cluster independently, but despite the selection
707 predispositions imposed by each method, a core of EV associated proteins and lipids was
708 detectable using all the approaches.

709 **Acknowledgments**

710 DP acknowledges his funding from the Department of Pharmacology, the Alison Brading
711 Memorial Fund Lady Margaret Hall, the Clarendon Fund provided by the University of Oxford
712 and the Medical Research Council (MR/N013468/1). NA and RC acknowledge support by
713 research grants from the British Heart Foundation (BHF) Centre of Research Excellence,
714 Oxford (NA and RC: RE/13/1/30181 and RE/18/3/34214); British Heart Foundation Project
715 Grant (NA and RC: PG/18/53/33895); the Tripartite Immunometabolism Consortium, Novo
716 Nordisk Foundation (RC: NNF15CC0018486); Oxford Biomedical Research Centre (BRC);
717 Nuffield Benefaction for Medicine and the Wellcome Institutional Strategic Support Fund
718 (ISSF) (NA) and a Health Research Bridging Salary Scheme (HRBSS) to N.A. BZ work was
719 supported by funding from the European Union's Horizon 2020 Research and Innovation
720 Program under Marie Skłodowska-Curie Grant Agreement 812890, ArthritisHeal. The views
721 expressed are those of the author(s) and not necessarily those of the National Health
722 Service, the National Institutes of Health Research or the Department of Health

723

724 **Declaration statement**

725 The Author(s) declare(s) that there is no conflict of interest.

726 **References**

- 727 1. de Miguel Pérez, D., et al., Extracellular vesicle-miRNAs as liquid biopsy biomarkers
728 for disease identification and prognosis in metastatic colorectal cancer patients. *Sci Rep*,
729 2020. 10(1): p. 3974.
- 730 2. Dong, L., et al., Circulating Long RNAs in Serum Extracellular Vesicles: Their
731 Characterization and Potential Application as Biomarkers for Diagnosis of Colorectal Cancer.
732 *Cancer Epidemiol Biomarkers Prev*, 2016. 25(7): p. 1158-66.
- 733 3. Burrello, J., et al., Sphingolipid composition of circulating extracellular vesicles after
734 myocardial ischemia. *Sci Rep*, 2020. 10(1): p. 16182.
- 735 4. Kalani, M.Y.S., et al., Extracellular microRNAs in blood differentiate between
736 ischaemic and haemorrhagic stroke subtypes. *J Extracell Vesicles*, 2020. 9(1): p. 1713540.
- 737 5. Akbar, N., et al., Endothelium-derived extracellular vesicles promote splenic
738 monocyte mobilization in myocardial infarction. *JCI Insight*, 2017. 2(17).
- 739 6. Akbar, N., et al., Rapid neutrophil mobilisation by VCAM-1+ endothelial extracellular
740 vesicles. *Cardiovasc Res*, 2022.
- 741 7. Evander, M., et al., Non-contact acoustic capture of microparticles from small plasma
742 volumes. *Lab Chip*, 2015. 15(12): p. 2588-96.
- 743 8. Kowal, J., et al., Proteomic comparison defines novel markers to characterize
744 heterogeneous populations of extracellular vesicle subtypes. *Proc Natl Acad Sci U S A*,
745 2016. 113(8): p. E968-77.
- 746 9. Onódi, Z., et al., Isolation of High-Purity Extracellular Vesicles by the Combination of
747 Iodixanol Density Gradient Ultracentrifugation and Bind-Elute Chromatography From Blood
748 Plasma. *Front Physiol*, 2018. 9: p. 1479.
- 749 10. Nordin, J.Z., et al., Ultrafiltration with size-exclusion liquid chromatography for high
750 yield isolation of extracellular vesicles preserving intact biophysical and functional properties.
751 *Nanomedicine*, 2015. 11(4): p. 879-83.
- 752 11. Geyer, P.E., et al., Plasma Proteome Profiling to detect and avoid sample-related
753 biases in biomarker studies. *EMBO Mol Med*, 2019. 11(11): p. e10427.

- 754 12. Brennan, K., et al., A comparison of methods for the isolation and separation of
755 extracellular vesicles from protein and lipid particles in human serum. *Scientific Reports*,
756 2020. 10(1): p. 1039.
- 757 13. Van Deun, J., et al., The impact of disparate isolation methods for extracellular
758 vesicles on downstream RNA profiling. *J Extracell Vesicles*, 2014. 3.
- 759 14. They, C., et al., Minimal information for studies of extracellular vesicles 2018
760 (MISEV2018): a position statement of the International Society for Extracellular Vesicles and
761 update of the MISEV2014 guidelines. *J Extracell Vesicles*, 2018. 7(1): p. 1535750.
- 762 15. Tian, Y., et al., Quality and efficiency assessment of six extracellular vesicle isolation
763 methods by nano-flow cytometry. *J Extracell Vesicles*, 2020. 9(1): p. 1697028.
- 764 16. Veerman, R.E., et al., Molecular evaluation of five different isolation methods for
765 extracellular vesicles reveals different clinical applicability and subcellular origin. *Journal of*
766 *Extracellular Vesicles*, 2021. 10(9): p. e12128.
- 767 17. de Menezes-Neto, A., et al., Size-exclusion chromatography as a stand-alone
768 methodology identifies novel markers in mass spectrometry analyses of plasma-derived
769 vesicles from healthy individuals. *J Extracell Vesicles*, 2015. 4: p. 27378.
- 770 18. Gidlöf, O., et al., Proteomic profiling of extracellular vesicles reveals additional
771 diagnostic biomarkers for myocardial infarction compared to plasma alone. *Sci Rep*, 2019.
772 9(1): p. 8991.
- 773 19. Askeland, A., et al., Mass-Spectrometry Based Proteome Comparison of
774 Extracellular Vesicle Isolation Methods: Comparison of ME-kit, Size-Exclusion
775 Chromatography, and High-Speed Centrifugation. *Biomedicines*, 2020. 8(8): p. 246.
- 776 20. Palviainen, M., et al., Extracellular vesicles from human plasma and serum are
777 carriers of extravesicular cargo-Implications for biomarker discovery. *PLoS One*, 2020.
778 15(8): p. e0236439.
- 779 21. Cao, F., et al., Proteomics comparison of exosomes from serum and plasma
780 between ultracentrifugation and polymer-based precipitation kit methods. *Electrophoresis*,
781 2019. 40(23-24): p. 3092-3098.

- 782 22. Jung, H.H., et al., Cytokine profiling in serum-derived exosomes isolated by different
783 methods. *Scientific Reports*, 2020. 10(1): p. 14069.
- 784 23. Stranska, R., et al., Comparison of membrane affinity-based method with size-
785 exclusion chromatography for isolation of exosome-like vesicles from human plasma.
786 *Journal of Translational Medicine*, 2018. 16(1): p. 1.
- 787 24. Gutiérrez García, G., et al., Analysis of RNA yield in extracellular vesicles isolated by
788 membrane affinity column and differential ultracentrifugation. *PLoS One*, 2020. 15(11): p.
789 e0238545.
- 790 25. Peterka, O., et al., Lipidomic characterization of exosomes isolated from human
791 plasma using various mass spectrometry techniques. *Biochim Biophys Acta Mol Cell Biol*
792 *Lipids*, 2020. 1865(5): p. 158634.
- 793 26. Shtam, T., et al., Evaluation of immune and chemical precipitation methods for
794 plasma exosome isolation. *PLoS One*, 2020. 15(11): p. e0242732.
- 795 27. Welton, J.L., et al., Ready-made chromatography columns for extracellular vesicle
796 isolation from plasma. *J Extracell Vesicles*, 2015. 4: p. 27269.
- 797 28. Thompson, A.G., et al., CSF extracellular vesicle proteomics demonstrates altered
798 protein homeostasis in amyotrophic lateral sclerosis. *Clin Proteomics*, 2020. 17: p. 31.
- 799 29. Subedi, P., et al., Comparison of methods to isolate proteins from extracellular
800 vesicles for mass spectrometry-based proteomic analyses. *Anal Biochem*, 2019. 584: p.
801 113390.
- 802 30. Mi, H., et al., PANTHER version 14: more genomes, a new PANTHER GO-slim and
803 improvements in enrichment analysis tools. *Nucleic Acids Res*, 2019. 47(D1): p. D419-D426.
- 804 31. Kim, D.K., et al., EVpedia: an integrated database of high-throughput data for
805 systemic analyses of extracellular vesicles. *J Extracell Vesicles*, 2013. 2.
- 806 32. Kalra, H., et al., Vesiclepedia: a compendium for extracellular vesicles with
807 continuous community annotation. *PLoS Biol*, 2012. 10(12): p. e1001450.
- 808 33. Simpson, R.J., H. Kalra, and S. Mathivanan, ExoCarta as a resource for exosomal
809 research. *J Extracell Vesicles*, 2012. 1.

- 810 34. Jorgensen, M., et al., Extracellular Vesicle (EV) Array: microarray capturing of
811 exosomes and other extracellular vesicles for multiplexed phenotyping. *J Extracell Vesicles*,
812 2013. 2.
- 813 35. Akawi, N., et al., Fat-Secreted Ceramides Regulate Vascular Redox State and
814 Influence Outcomes in Patients With Cardiovascular Disease. *Journal of the American*
815 *College of Cardiology*, 2021. 77(20): p. 2494-2513.
- 816 36. Serrano-Pertierra, E., et al., Characterization of Plasma-Derived Extracellular
817 Vesicles Isolated by Different Methods: A Comparison Study. *Bioengineering (Basel)*, 2019.
818 6(1).
- 819 37. Gámez-Valero, A., et al., Size-Exclusion Chromatography-based isolation minimally
820 alters Extracellular Vesicles' characteristics compared to precipitating agents. *Sci Rep*, 2016.
821 6: p. 33641.
- 822 38. Webber, J. and A. Clayton, How pure are your vesicles? *J Extracell Vesicles*, 2013.
823 2.
- 824 39. Théry, C., et al., Minimal information for studies of extracellular vesicles 2018
825 (MISEV2018): a position statement of the International Society for Extracellular Vesicles and
826 update of the MISEV2014 guidelines. *J Extracell Vesicles*, 2018. 7(1): p. 1535750.
- 827 40. Skotland, T., et al., An emerging focus on lipids in extracellular vesicles. *Adv Drug*
828 *Deliv Rev*, 2020. 159: p. 308-321.
- 829 41. Karimi, N., et al., Detailed analysis of the plasma extracellular vesicle proteome after
830 separation from lipoproteins. *Cell Mol Life Sci*, 2018. 75(15): p. 2873-2886.
- 831 42. Yuana, Y., et al., Co-isolation of extracellular vesicles and high-density lipoproteins
832 using density gradient ultracentrifugation. *J Extracell Vesicles*, 2014. 3.
- 833 43. Gidlof, O., et al., Proteomic profiling of extracellular vesicles reveals additional
834 diagnostic biomarkers for myocardial infarction compared to plasma alone. *Sci Rep*, 2019.
835 9(1): p. 8991.
- 836 44. Bæk, R. and M.M. Jørgensen, Multiplexed Phenotyping of Small Extracellular
837 Vesicles Using Protein Microarray (EV Array). *Methods Mol Biol*, 2017. 1545: p. 117-127.

- 838 45. Tóth, E., et al., Formation of a protein corona on the surface of extracellular vesicles
839 in blood plasma. *J Extracell Vesicles*, 2021. 10(11): p. e12140.
- 840 46. Tian, B.M., et al., Human platelet lysate supports the formation of robust human
841 periodontal ligament cell sheets. *J Tissue Eng Regen Med*, 2018. 12(4): p. 961-972.
- 842 47. Mathieu, M., et al., Specificities of exosome versus small ectosome secretion
843 revealed by live intracellular tracking of CD63 and CD9. *Nat Commun*, 2021. 12(1): p. 4389.
- 844 48. Martínez-Beamonte, R., et al., Sphingomyelin in high-density lipoproteins: structural
845 role and biological function. *Int J Mol Sci*, 2013. 14(4): p. 7716-41.
- 846 49. Sódar, B.W., et al., Low-density lipoprotein mimics blood plasma-derived exosomes
847 and microvesicles during isolation and detection. *Sci Rep*, 2016. 6: p. 24316.
- 848 50. Izzo, C., F. Grillo, and E. Murador, Improved method for determination of high-
849 density-lipoprotein cholesterol I. Isolation of high-density lipoproteins by use of polyethylene
850 glycol 6000. *Clin Chem*, 1981. 27(3): p. 371-4.
- 851 51. Simonsen, J.B., What Are We Looking At? Extracellular Vesicles, Lipoproteins, or
852 Both? *Circ Res*, 2017. 121(8): p. 920-922.
- 853

854 **Figures**

855 **Figure 1: A methodological overview.** Platelet poor plasma was obtained from healthy
856 volunteers (n=4) and patients presenting with myocardial infarction (MI) (n=6) (and from the
857 same patients 1-month post-MI) and plasma extracellular vesicles (EV) isolated using five
858 different methods: ultracentrifugation (UC), precipitation, acoustic trapping, size exclusion
859 chromatography (SEC) and immunoaffinity capture with a matched vehicle phosphate
860 buffered saline (PBS) or IgG control. The plasma EV were analyzed using Nanoparticle
861 Tracking Analysis, protein concentration, Western blot, transmission electron microscopy, a
862 targeted EV-protein array for EV-markers CD9, CD63, CD81, ALIX, TSG101, flotillin,
863 Annexin V and 18 other cell associated markers, untargeted proteomics (LC-MS/MS) and
864 targeted sphingolipidomics (LC-MS/MS). The data were analyzed in insolation and following
865 integrated hierarchical clustering and principal component analysis.

866

867 **Figure 2: Plasma EV characterization using different isolation methods. (A)** Total
868 plasma extracellular vesicles (EV) / mL concentrations and **(B)** size and concentration
869 distribution profiles were obtained by Nanoparticle Tracking Analysis (NTA) using
870 ultracentrifugation (UC), precipitation, acoustic trapping, size exclusion chromatography
871 (SEC) and immunoaffinity capture (n=4). Values are presented as a delta compared to a
872 vehicle control or IgG control. Scale is logarithmic. **(C)** Protein concentration of plasma EV
873 using UC, precipitation, acoustic trapping, SEC and immunoaffinity capture (n=4). Values
874 are presented as a delta compared to a vehicle control or IgG control. **(D)** Western blot of
875 plasma EV derived from UC, precipitation, acoustic trapping, SEC and immunoaffinity
876 capture versus controls using EV markers ALIX and CD63, lipoprotein contaminants
877 apolipoprotein B (ApoB), and apolipoprotein A-I (ApoA-I), plasma contaminant albumin and
878 cellular contaminant histone H3. Endothelial cell EV and Peripheral blood mononuclear cells
879 (PBMCs) were used for H3 positive controls. **(E-J).** Transmission electron microscopy (TEM)
880 images of isolated plasma EV from UC, precipitation, acoustic trapping, SEC and
881 immunoaffinity capture versus controls. Each sub panel contains a zoomed-in image (left

882 image), an overview image (top right) and a control vehicle image (bottom right). For the
883 immunoaffinity bead capture images, the red arrows indicate EV particles. The scale bar is
884 200 nm for the zoomed images surrounded by a dashed line and 1000 nm for the overview
885 images and **J**. Values in **A** and **C** are group average \pm standard deviation (SD). Data are
886 group average \pm standard deviation (SD) (n=6).

887 Data was analyzed by one-way ANOVA with post-hoc Bonferroni correction. ***p<0.001.

888

889 **Figure 3: Heatmap of plasma EV derived from different isolation methods using the**
890 **EV- protein-Array.** The heatmap contains extracellular vesicles (EV) markers CD9, CD81,
891 CD63, ALIX, TSG101, Flotillin 1 and Annexin V for ultracentrifugation (UC), precipitation,
892 acoustic trapping, size exclusion chromatography (SEC) and immunoaffinity capture, lipid
893 contaminants apolipoprotein H (ApoH) and apolipoprotein E (ApoE) and cell associated
894 markers. Values are presented as a delta compared to a vehicle control or IgG control and
895 are log normalized (n=4 per isolation method). Data was analyzed by Kruskal-Wallis test
896 with post-hoc Bonferroni correction. *p<0.05, ***p<0.001.

897

898 **Figure 4: Proteomic comparison of plasma EV isolation methods. (A)** The number of
899 protein groups quantified by unbiased proteomics for plasma extracellular vesicles (EV)
900 derived by: ultracentrifugation (UC), precipitation, acoustic trapping, size exclusion
901 chromatography (SEC) and immunoaffinity capture, versus control vehicle (PBS) or an IgG
902 control. Protein groups were only included as quantified if they had ≥ 2 unique peptides.
903 (n=3-4). One-way ANOVA with post-hoc Bonferroni correction. Data are group averages \pm
904 standard deviation (SD). *p<0.05, ***p<0.001. **(B)** A heatmap of the top 30 quantified protein
905 groups across all isolation methods. Values from control samples were subtracted to
906 account for background and the values were log normalised. Hierarchical clustering of the
907 isolation methods was conducted using a complete clustering method. (n=3-4).

908

909 **Figure 5: Sphingolipidomic analysis of plasma EV from different isolation methods.**

910 **(A)** Number of sphingolipids quantified in plasma extracellular vesicles (EV) isolated by
911 ultracentrifugation (UC), precipitation, acoustic trapping, size-exclusion chromatography
912 (SEC) and immunoaffinity capture and subjected to targeted sphingolipid analysis versus
913 control vehicle (PBS) or an IgG control. Data are group averages \pm standard deviation (SD)
914 and were analysed by One-way ANOVA with post-hoc Bonferroni correction. *** $p < 0.001$.
915 (n=4) **(B)** Heat map of plasma EV sphingolipids. Values from control samples were
916 subtracted to account for background and the values were log normalised. Hierarchical
917 clustering of the isolation methods was conducted using a complete clustering method. (n=3-
918 4). Data were analysed by Kruskal-Wallis test with post-hoc Bonferroni correction.

919

920 **Figure 6: Principal component analysis of plasma EV characteristics following data**

921 **integration. (A)** A principal component (PC) analysis of plasma extracellular vesicles (EV)
922 isolated by ultracentrifugation (UC), precipitation, acoustic trapping, size-exclusion
923 chromatography (SEC) and immunoaffinity capture: including plasma EV concentration,
924 protein concentration, EV-protein-Array, proteomics and sphingolipidomics. The integrated
925 data was condensed to PC1 and PC2. **(B)** A heatmap with the various principal components
926 to compare the different isolation plasma EV isolation methods. Hierarchical clustering of the
927 isolation methods was conducted using a complete clustering method. (n=3-4).

928

929 **Figure 7: Plasma EV analysis using different isolation methods in patients following**

930 **presentation with myocardial (MI) infarction compared to samples from the same**

931 **patients after a 1-month follow up. (A)** Comparison of concentration and size-distribution

932 profile by Nanoparticle Tracking Analysis of plasma extracellular vesicles (EV) from patients

933 following presentation with MI and after a 1-month follow up using: ultracentrifugation (UC),

934 precipitation, acoustic trapping, size exclusion chromatography (SEC) and immunoaffinity

935 capture (n=6 per timepoint). Data are group average \pm standard deviation (SD). Paired T-

936 test analysis * $p < 0.05$. **(B)** A Pearson correlation analysis of plasma EV / mL derived from

937 each isolation method at time of presentation vs. the infarct size determined by cardiac MRI
938 using late gadolinium enhancement 6-months post-infarct (n=5). **(C)** Heatmap of plasma EV-
939 Array analysis. The top section of the heatmap contains the different EV markers CD9,
940 CD81, CD63, ALIX, TSG101, Flotillin 1 and Annexin V. Values are presented as fold over
941 the respective matched follow up control sample. **(D)** Heatmap showing the plasma EV
942 sphingolipidomic profiles in MI patients at presentation versus a 1-month follow up for UC,
943 precipitation, acoustic trapping, SEC and immunoaffinity capture. Values are presented as
944 fold over the respective matched follow up.

945

946 **Figure 8: Principal component analysis of integrated plasma EV characterisation at**
947 **time of presentation with myocardial infarction (MI) vs. 1-month follow-up in the same**
948 **patients using different plasma EV isolation methods.** A principal component (PC)
949 analysis of plasma EV isolated by ultracentrifugation (UC), precipitation, acoustic trapping,
950 size-exclusion chromatography (SEC) and immunoaffinity capture from patients presenting
951 with MI versus a 1-month follow up control. Plasma EV characteristics include including
952 plasma EV concentration, protein concentration, EV-protein-Array and sphingolipidomics.
953 The integrated data was condensed to PC1 and PC2. (n=5-6). The eclipses indicate the
954 95% confidence interval.

955

956 **Tables**

957 **Table 1: Nanoparticle Tracking Analysis showing the mean and median size of**
958 **plasma- EV** isolated by ultracentrifugation (UC), precipitation, acoustic trapping, size-
959 exclusion chromatography (SEC). Immunoaffinity capture can not be acquired. Data are
960 group averages \pm standard deviation (SD) and were analyzed by One-way ANOVA with
961 post-hoc Bonferroni correction. *** $p < 0.001$. (n=4).

962

963 **Table 2: Clinical characteristics of the MI patients.** Age, sex (M/F), glucose, white blood
964 cells counts, troponin peak, cholesterol, diabetes status, smoker status, infarct size
965 determined by late gadolinium enhancement MRI 6 months post-AMI and left ventricle
966 ejection fraction (LVEF %) 6 months post-MI. Data are group averages \pm standard deviation
967 (SD) (n=6).

968 **Supplemental Figures**

969 **Supplemental Figure 1: The ratio of plasma extracellular vesicles (EV) to protein**
970 **concentration per isolation method:** ultracentrifugation (UC), precipitation, acoustic
971 trapping, size-exclusion chromatography (SEC) and immunoaffinity capture. EV are
972 expressed as per mL and protein concentration is expressed μg . Values are expressed as
973 delta over phosphate buffer solution (PBS) control or IgG control. Data are group averages \pm
974 standard deviation (SD) (n=4). One-way ANOVA with post-hoc Bonferroni correction.
975 **p<0.01, ***p<0.001.

976

977 **Supplemental Figure 2: Venn diagram of quantified protein groups in different plasma**
978 **extracellular vesicle (EV) isolation methods:** ultracentrifugation (UC), precipitation,
979 acoustic trapping, size-exclusion chromatography (SEC) and immunoaffinity capture.
980 Quantified protein groups within a method were pooled after subtraction of phosphate buffer
981 solution (PBS) control or IgG control. Protein groups that had more than 1 repeat within a
982 method were included in the Venn diagram.

983

984 **Supplemental Figure 3: Gene Ontology analysis of plasma extracellular vesicle (EV)**
985 **isolation method proteomics:** ultracentrifugation (UC), precipitation, acoustic trapping,
986 size-exclusion chromatography (SEC) and immunoaffinity capture. **(A)** Quantified protein
987 groups were expressed as delta over phosphate buffer solution (PBS) control or IgG control.
988 Quantified protein groups that appeared more than once per method were included in the
989 Gene Ontology (GO) analysis. The GO cellular components associated with each method
990 were ranked based on the false discovery rate (FDR) and the top five were included in the
991 tables. In addition, the GO enrichment scores were plotted against the false discovery rate p-
992 values in the scatterplot. **(B)** The overlap between quantified protein groups per plasma EV
993 isolation method and published EV proteomics databases EVpedia, Exocarta and
994 Vesiclepedia. The table contains the percentage of overlapping protein groups vs. total
995 protein groups per isolation method, with a p-value calculated by fisher-exact test.

996

997 **Supplemental Figure 4: The overlap between the number of quantified protein groups**
998 **per plasma extracellular vesicle (EV) isolation method and published plasma EV**
999 **proteomic datasets.** Quantified protein groups within a method were pooled after
1000 subtraction of phosphate buffer solution (PBS) control or IgG control. Protein groups that had
1001 more than 1 repeat within a method were included. Plasma EV-proteomes determined by
1002 ultracentrifugation (UC), precipitation, acoustic trapping, size-exclusion chromatography
1003 (SEC) and immunoaffinity capture were compared with published EV proteomic datasets.
1004 The overlap of protein groups between each method were compared and listed out of the
1005 total protein groups quantified.

1006

1007 **Supplemental Figure 5: Venn diagram showing the overlap between quantified**
1008 **sphingolipids in different plasma extracellular vesicles (EV) isolation methods:**
1009 ultracentrifugation (UC), precipitation, acoustic trapping, size-exclusion chromatography
1010 (SEC) and immunoaffinity capture. Sphingolipids within a method were pooled after
1011 subtraction of phosphate buffer solution (PBS) control or IgG control. Sphingolipids that had
1012 more than 1 repeat within a method were included in the Venn diagram.

1013

1014 **Supplemental Figure 6: Scree plots of each principal component following the**
1015 **integrated data analysis of plasma extracellular vesicle (EV) isolated with the different**
1016 **methods:** ultracentrifugation (UC), precipitation, acoustic trapping, size-exclusion
1017 chromatography (SEC) and immunoaffinity capture. Data from the acquired unbiased
1018 proteomics, targeted sphingolipidomics, EV-Array analysis and concentration/size analysis
1019 was pooled for each isolation method. Principal components were generated with the R-
1020 package *Factoextra* and *FactoMineR*. Each scree plot indicates the percentage of variance
1021 explained for the principal component and the top 30 drivers for the principal component.
1022 Data was labelled based on the origin; Lipid indicates data from the targeted sphingolipid

1023 data, EV indicates data from the EV-protein-array and unlabeled was selected for data from
1024 the proteomics.

1025

1026 **Supplemental Figure 7: Plasma extracellular vesicle (EV) concentration and size**
1027 **characteristics after isolation from myocardial infarction (MI) patients at time of**
1028 **presentation and one month follow up. (A)** The variance of plasma EV concentration
1029 isolated by each method measured by Nanoparticle Tracking Analysis (NTA). The variance
1030 was calculated by relative standard deviation over three different measurements. Values are
1031 expressed as delta over phosphate buffer solution (PBS) control or IgG control. **(B)** The
1032 average size of the isolated plasma EV for each method at time of presentation vs. follow up
1033 measured by NTA. Immunoaffinity capture can not be acquired. **(C)** Size distribution profiles
1034 of the plasma EV from MI patients at time of presentation and one month follow up.
1035 Immunoaffinity capture can not be acquired. Data are group averages \pm standard deviation
1036 (SD) (n=12 for **A**, n=6 for **B**, n=6 per time point for **C**). One-way ANOVA with post-hoc
1037 Bonferroni correction. *p<0.05 for **A** and **B**.

1038

1039 **Supplemental Figure 8: Sphingolipid concentrations of plasma extracellular vesicles**
1040 **(EV) isolated by different methods:** ultracentrifugation (UC), precipitation, acoustic
1041 trapping, size-exclusion chromatography (SEC) and immunoaffinity capture. The fold change
1042 in sphingolipid concentration in plasma EV isolated at time of presentation with myocardial
1043 infarction (MI) versus the concentration in plasma EV isolated 1-month post-MI per isolation
1044 method. Data are group averages \pm standard deviation (SD) and were analysed by one-way
1045 ANOVA with post-hoc Bonferroni correction. *p<0.05 and **p<0.01. (n=5-6)

1046

1047 **Supplemental Figure 9: Plasma extracellular vesicle (EV) sphingolipid concentration**
1048 **correlation with infarct size.** A Pearson correlation analysis was conducted with the the
1049 fold change in sphingolipid (**A**: Cer(d18:0/22:0) ; **B**: sphinganine (d18:0) ; **C**: SM(d18:1/18:1)
1050 concentration in plasma EV isolated at time of presentation with myocardial infarction (MI)

1051 versus the concentration in plasma EV isolated 1-month post-MI by the precipitation method
1052 versus the infarct size determined by cardiac MRI using late gadolinium enhancement 6-
1053 months post-infarct (n=5).

Figure 1

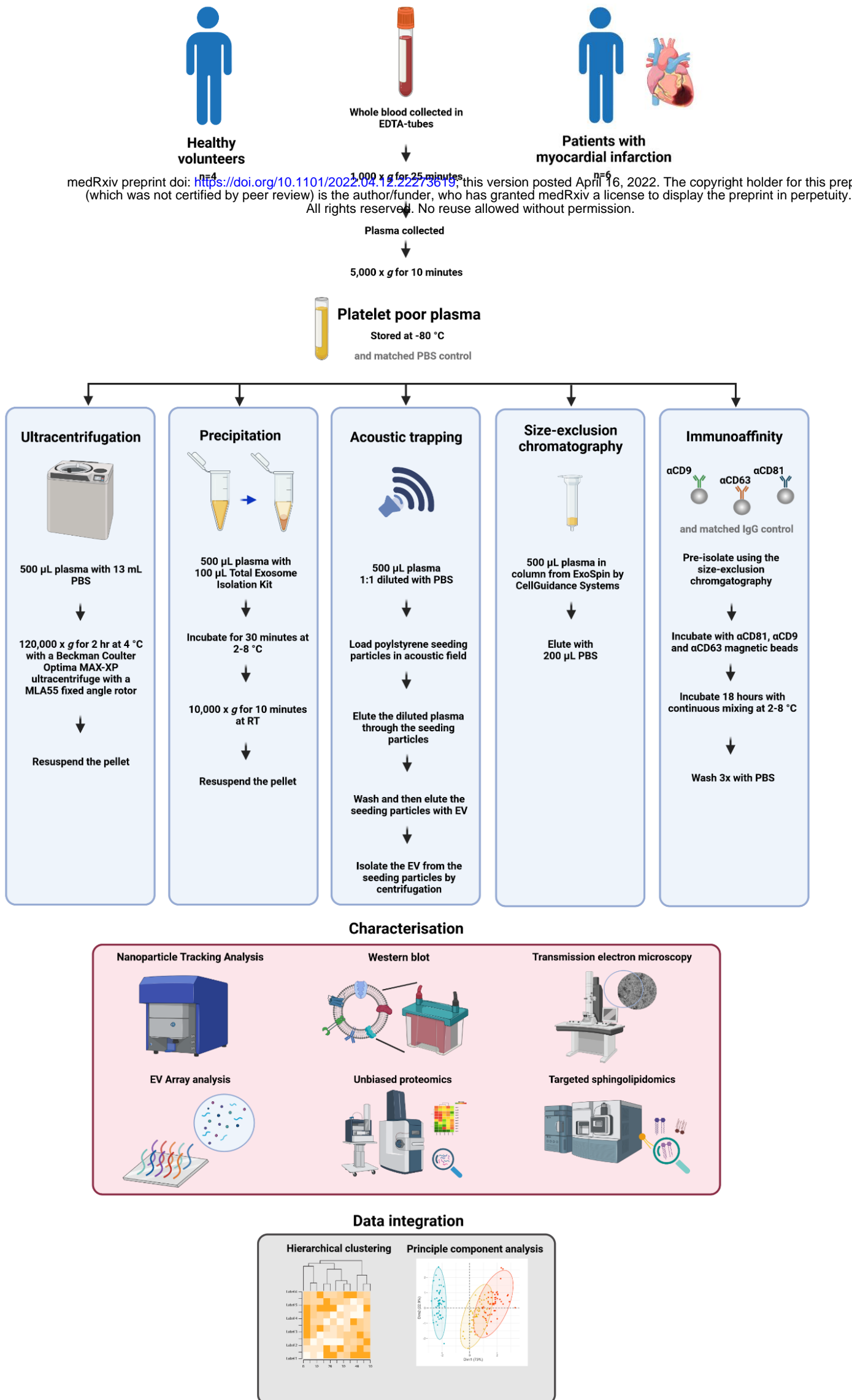


Figure 2

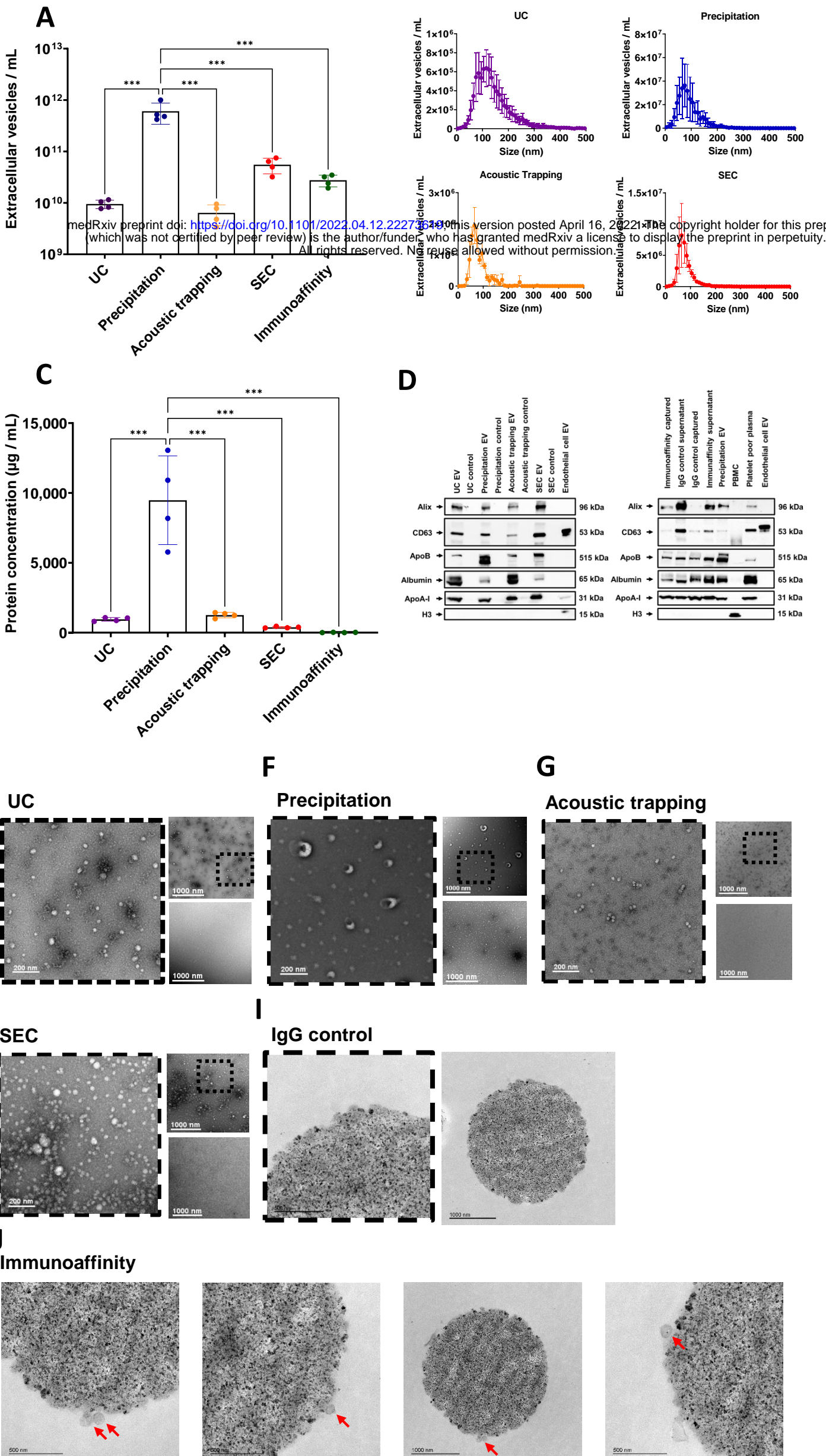


Figure 3

medRxiv preprint doi: <https://doi.org/10.1101/2022.04.12.22273619>; this version posted April 16, 2022. The copyright holder for this preprint (which was not certified by peer review) is the author/funder, who has granted medRxiv a license to display the preprint in perpetuity. All rights reserved. No reuse allowed without permission.

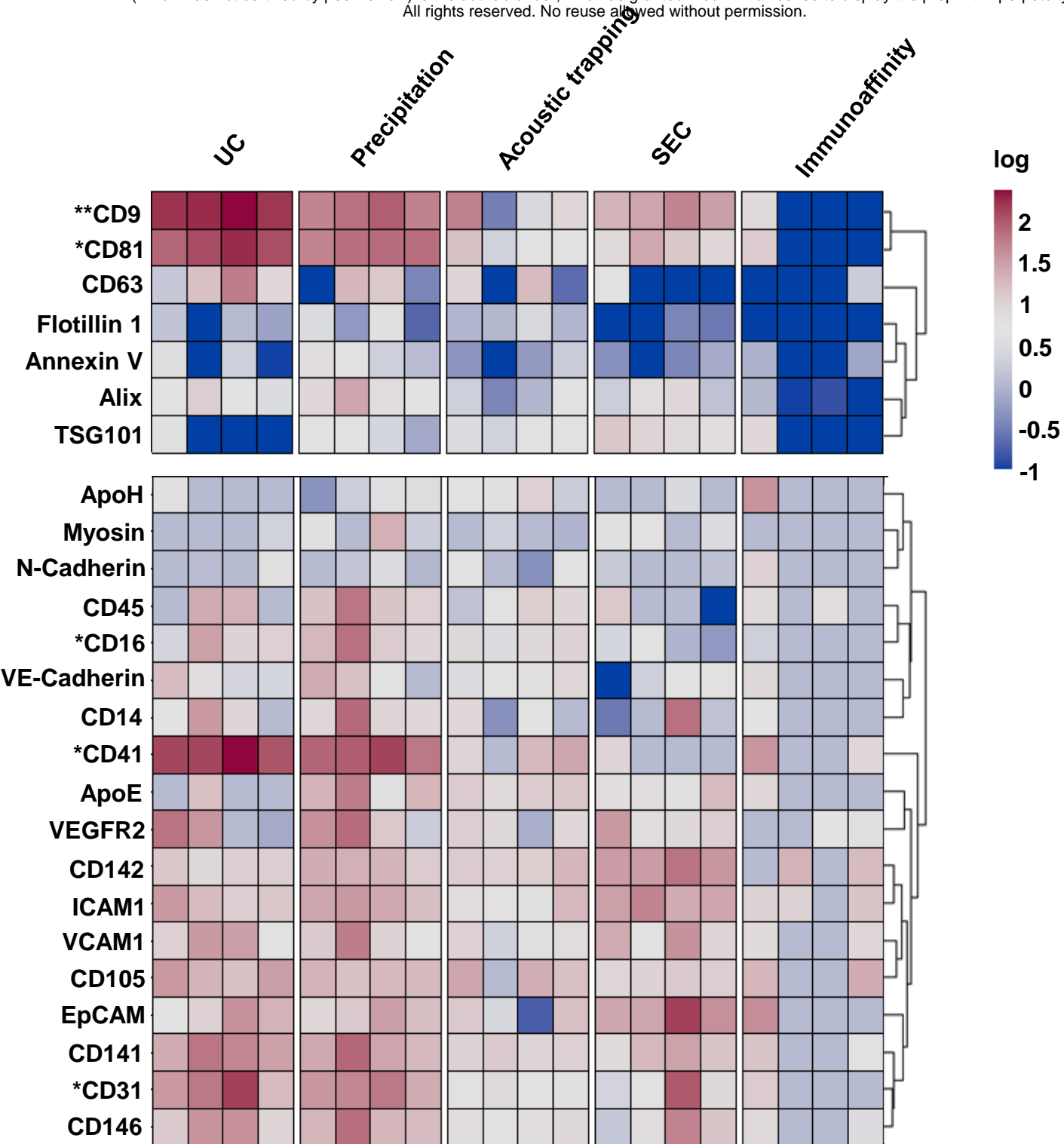


Figure 4

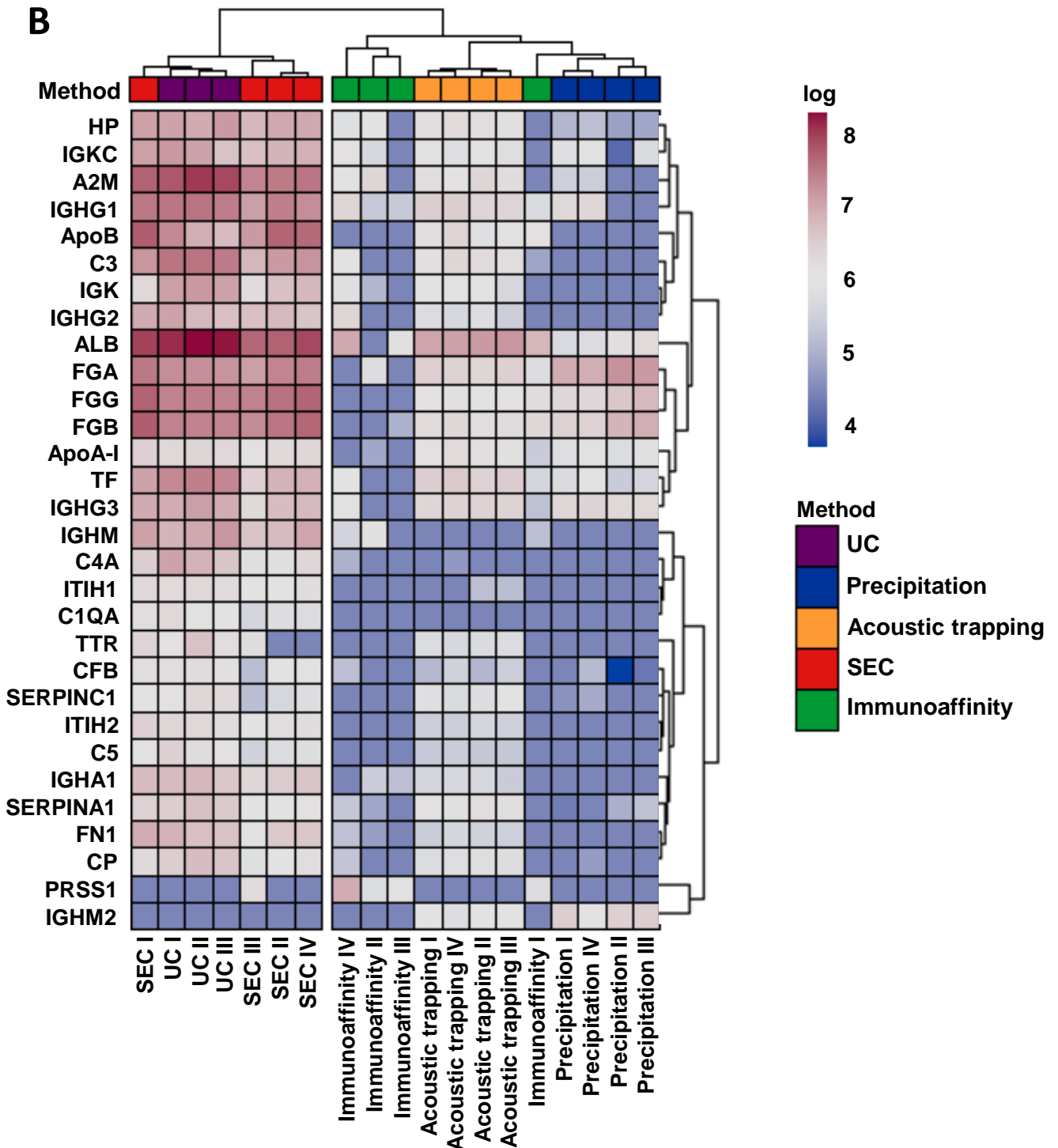
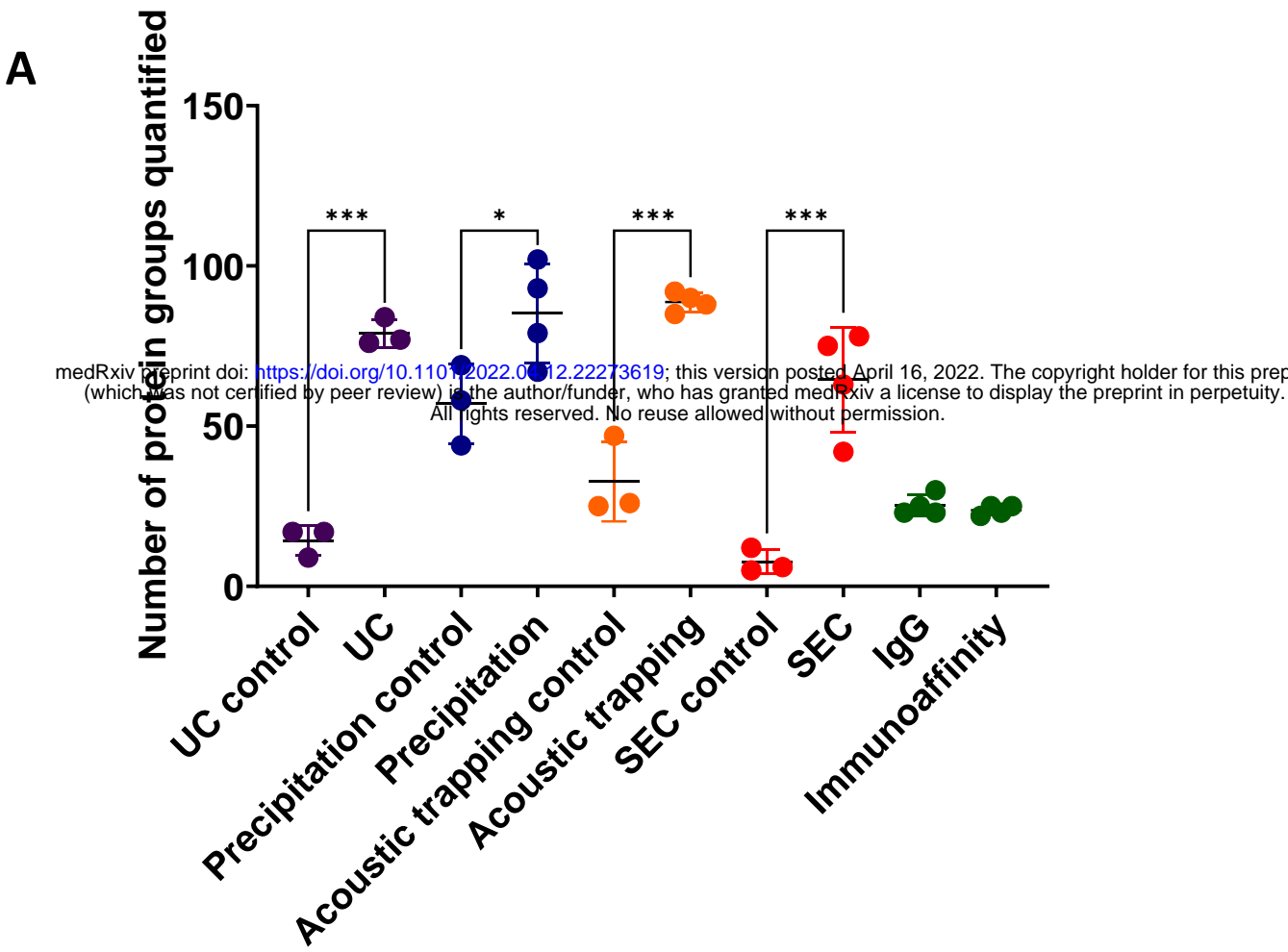
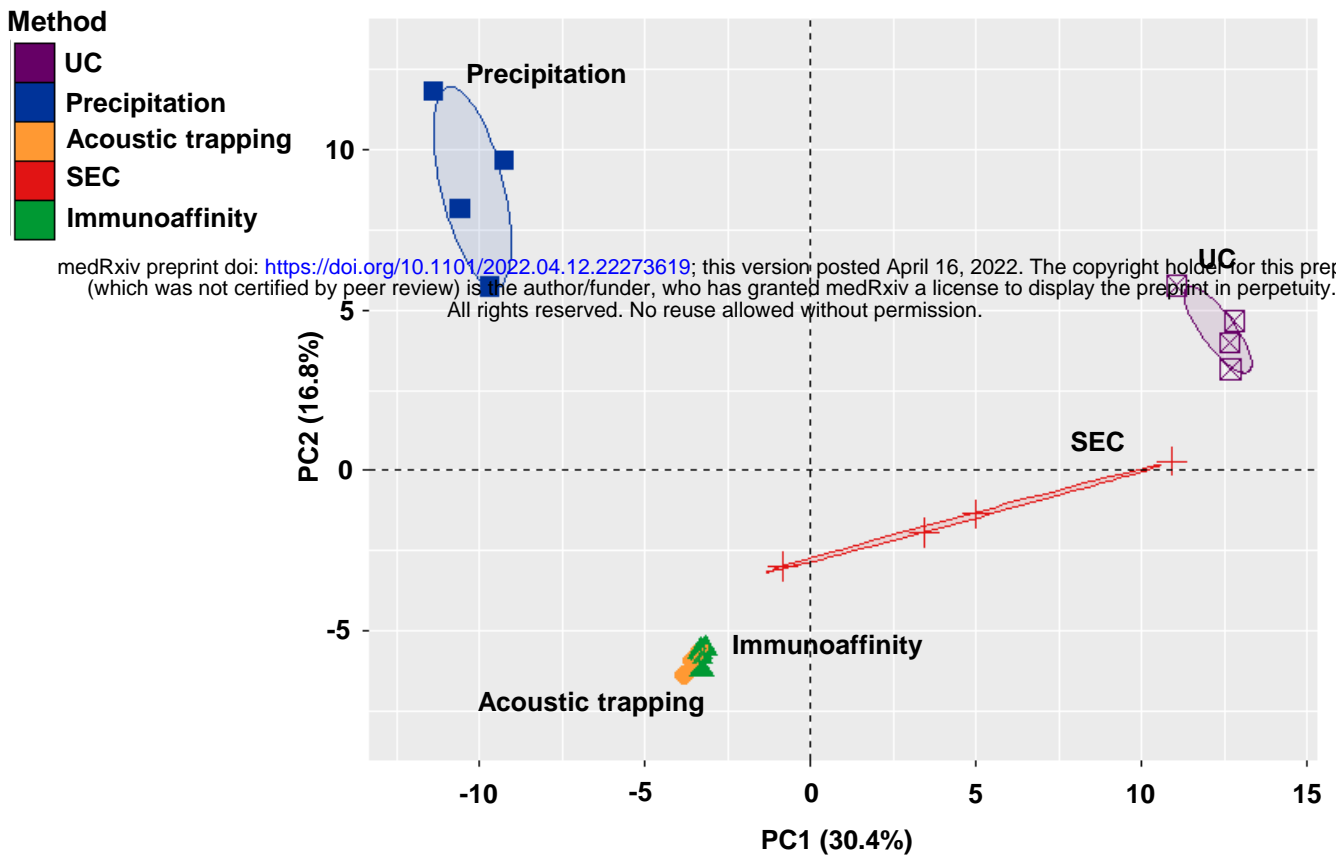


Figure 6

A



B

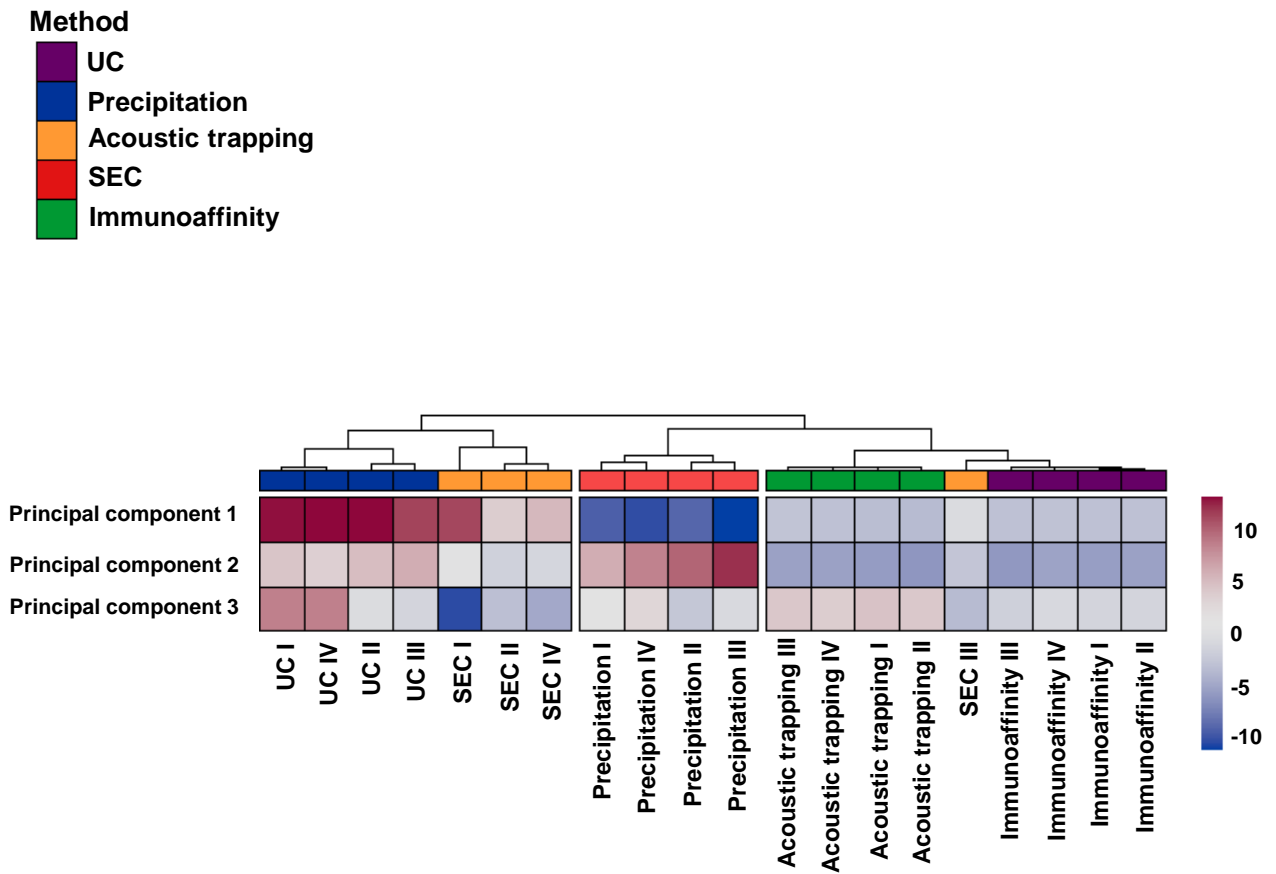
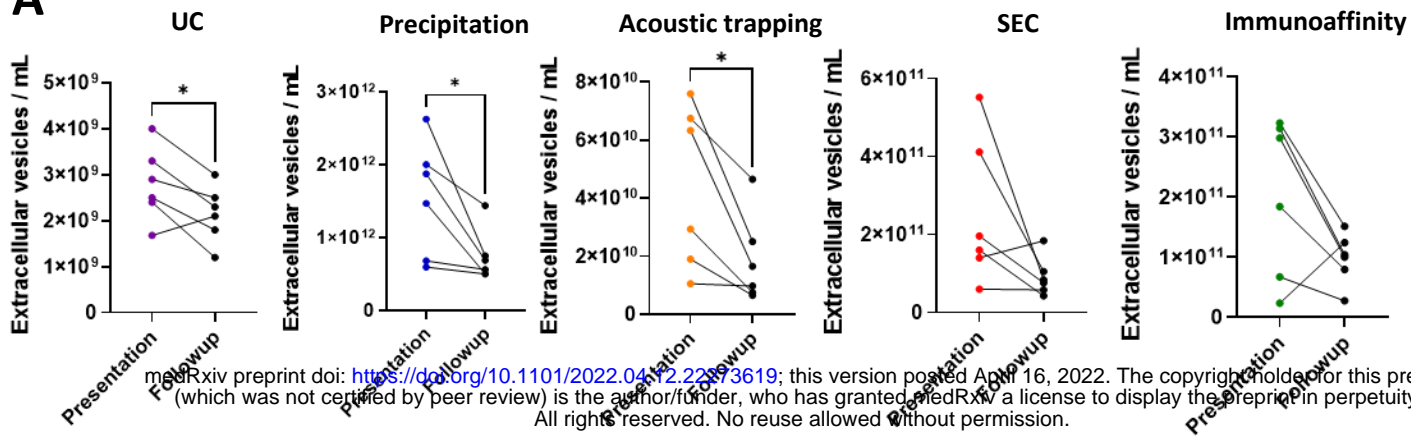
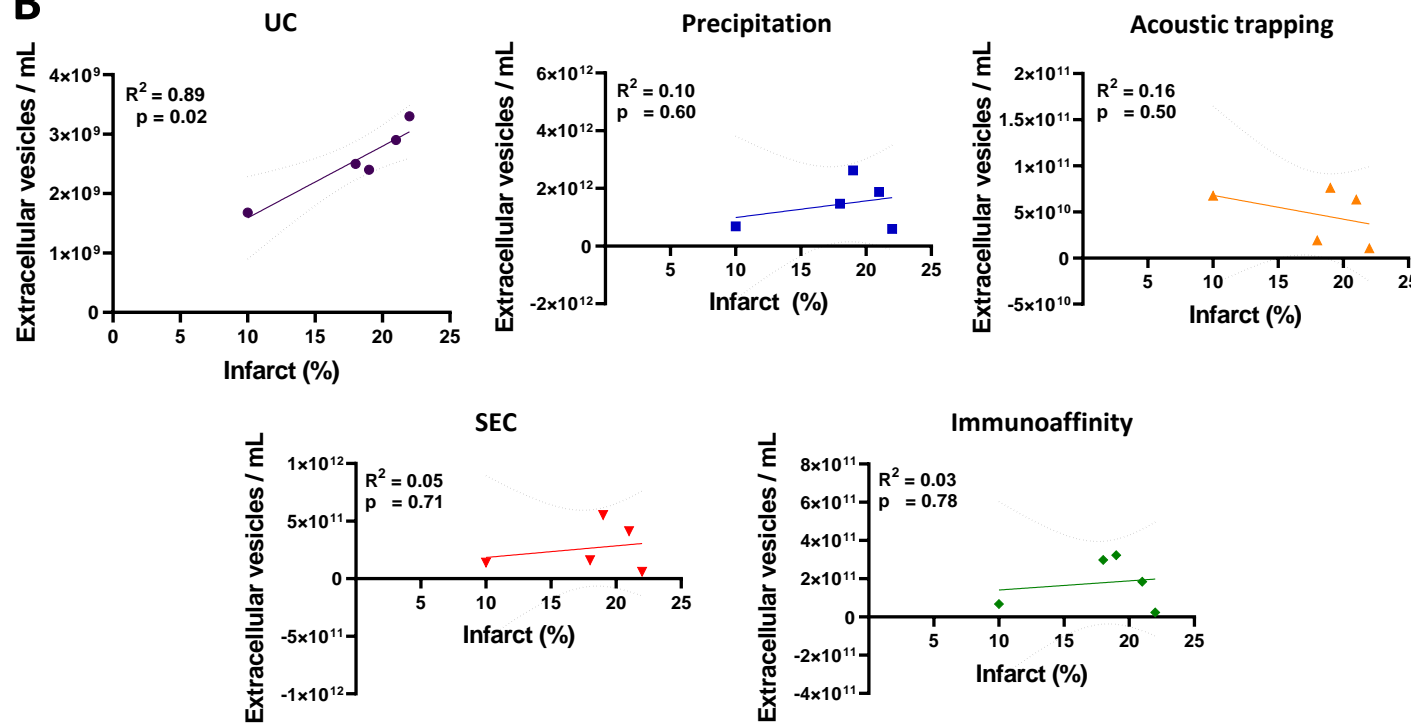


Figure 7

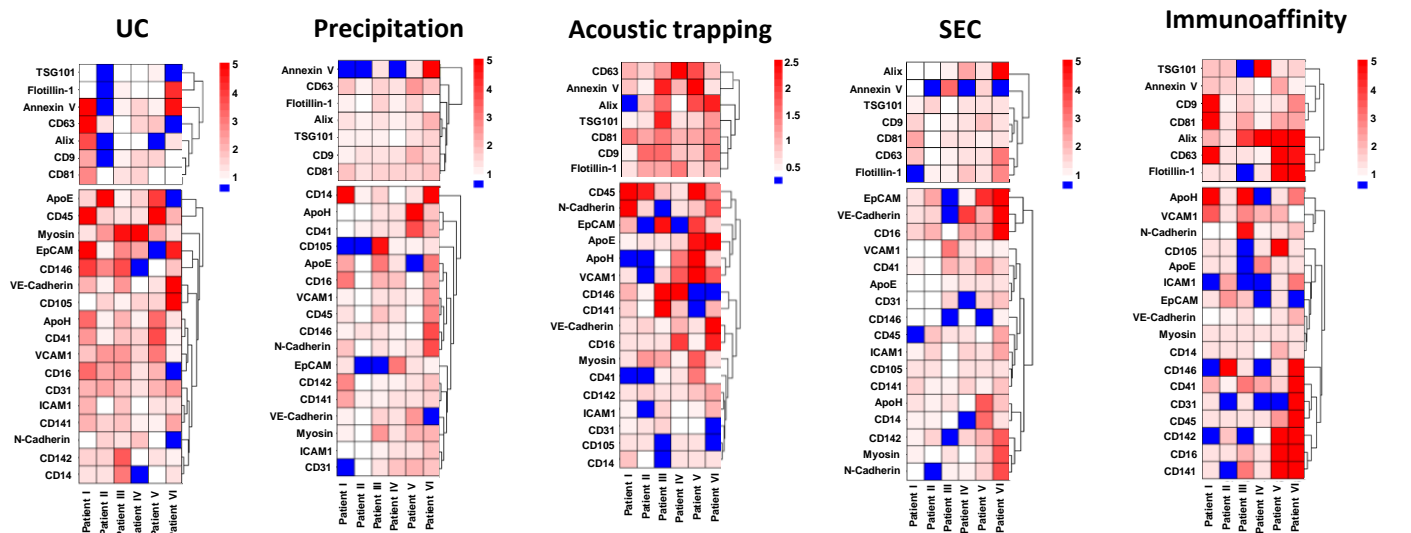
A



B



C



D

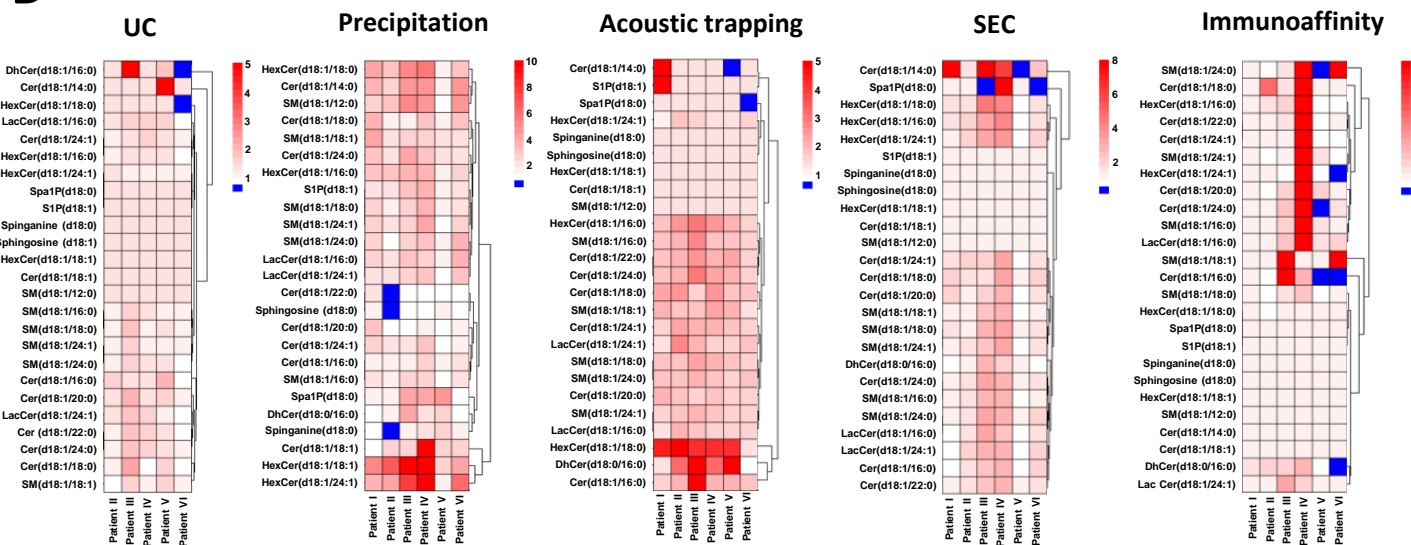
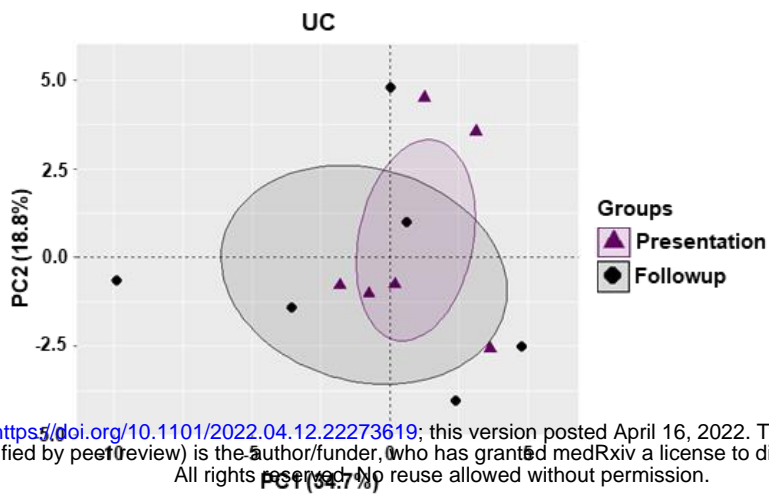


Figure 8



medRxiv preprint doi: <https://doi.org/10.1101/2022.04.12.22273619>; this version posted April 16, 2022. The copyright holder for this preprint (which was not certified by peer review) is the author/funder, who has granted medRxiv a license to display the preprint in perpetuity. All rights reserved. No reuse allowed without permission.

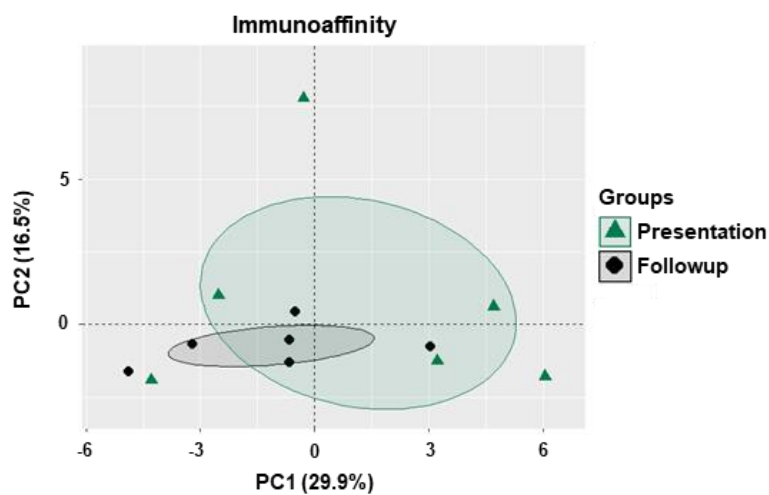
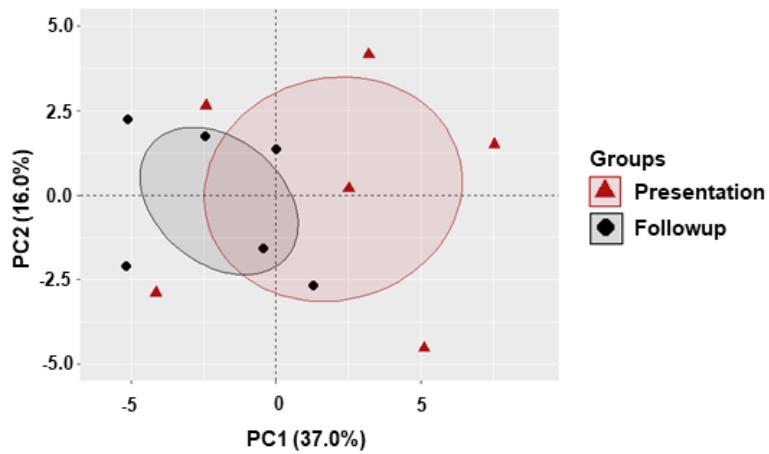
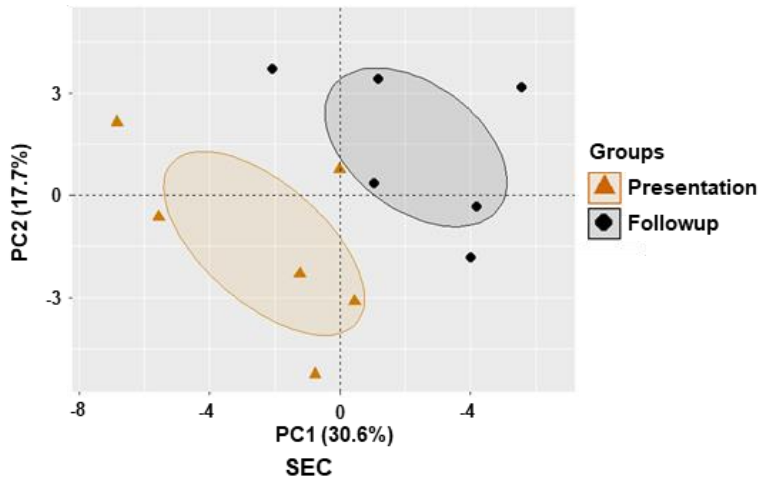
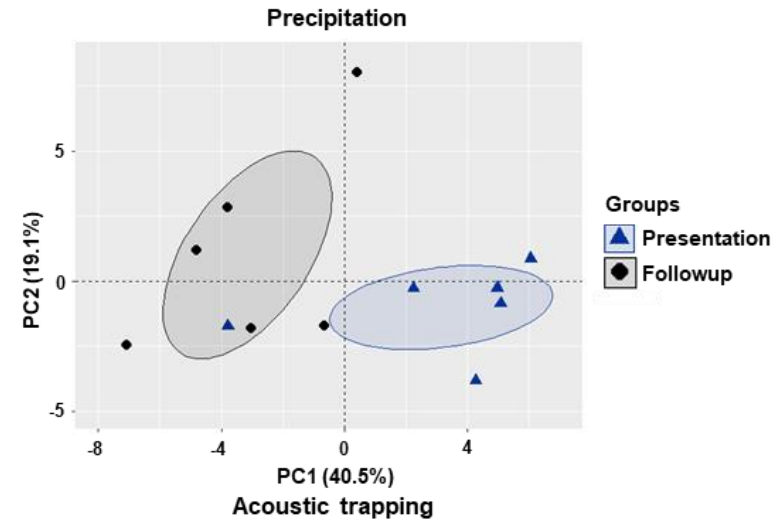


Table 1

	Mean size (nm)	Median size (nm)
***Ultracentrifugation	143.7 ± 3.4	125.0 ± 2.9
Precipitation	94.2 ± 3.9	84.0 ± 3.7
Acoustic trapping	81.2 ± 3.9	70.7 ± 4.6
SEC	87.2 ± 1.5	75.0 ± 1.4
Immunoaffinity	-	-

medRxiv preprint doi: <https://doi.org/10.1101/2022.04.12.22278619>; this version posted April 16, 2022. The copyright holder for this preprint (which was not certified by peer review) is the author/funder, who has granted medRxiv a license to display the preprint in perpetuity. All rights reserved. No reuse allowed without permission.

Table 2

	Average ± SD
Age	67.0 ± 11.4
Sex (male/female)	6/0
Glucose (mmol/L)	5.7 ± 0.5 (N=3)
White blood cell count (x10⁹)	7.6 ± 2.2
Troponin (peak ng/L) at presentation	358.7 ± 401.2
Cholesterol (mmol/L)	4.8 ± 1.2
Diabetic status (diabetes / non)	0/6
Smoker status (smoker / non)	1/5
Infarct size at 6-months	15 ± 7.8
LVEF at follow up (%)	47 ± 5.0

medRxiv preprint doi: <https://doi.org/10.1101/2022.04.12.22273619>; this version posted April 16, 2022. The copyright holder for this preprint (which was not certified by peer review) is the author/funder, who has granted medRxiv a license to display the preprint in perpetuity. All rights reserved. No reuse allowed without permission.